Accepted Manuscript

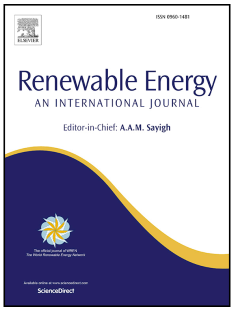

Series of detail comparison and optimization of thermoelectric element geometry considering the PV effect

Samson Shittu, Guiqiang Li, Xudong Zhao, Xiaoli Ma

PII: S0960-1481(18)30787-0

DOI: 10.1016/j.renene.2018.07.002

Reference: RENE 10276

To appear in: *Renewable Energy*

Received Date: 20 April 2018

Revised Date: 26 June 2018

Accepted Date: 2 July 2018

Please cite this article as: Shittu S, Li G, Zhao X, Ma X, Series of detail comparison and optimization of thermoelectric element geometry considering the PV effect, *Renewable Energy* (2018), doi: 10.1016/j.renene.2018.07.002.

Series of Detail Comparison and Optimization of Thermoelectric Element Geometry Considering the PV Effect

Samson Shittu[1], Guiqiang Li[1*], Xudong Zhao[1*], Xiaoli Ma[1]

[1] *School of Engineering, University of Hull, Hull HU6 7RX, UK*

Abstract

This study investigates the optimum geometry for maximum efficiency of a hybrid PV-TE uni-couple using Finite Element Method. COMSOL Multiphysics is used to solve the 3-Dimensional heat transfer equations considering thermoelectric materials with temperature dependent properties. Two types of thermoelectric element geometry area ratios are considered for the range $0.5 \le R_A \le 2$ and $0.5 \le R_S \le 2$. Nine different geometric configurations are analysed for two different PV cells. Effects of thermoelectric generator (TEG) geometric parameters, solar irradiation and concentration ratio on the hybrid system efficiency are presented. The results show that a hybrid PV-TE system will perform better with symmetrical TEG geometry ($R_A = R_S = 1$) if a PV temperature coefficient of 0.004/K (Cell B) is used. This is different from the optimum geometry for a TEG only system. However, the optimum geometry of the TEG in a hybrid system will be the same as that of a TEG only system (dissymmetrical i.e. $R_A = R_S \neq 1$) if a PV temperature coefficient of 0.001/K (Cell A) is used. The overall efficiency and TE temperature difference show a decreasing trend as thermoelectric element length and area increase respectively no matter the configuration or temperature coefficient value used. Results obtained from this research would influence hybrid PV-TE system design for obtaining maximum conversion efficiency.

Keywords: PV-TE, Finite Element Method, TE Area Ratio, Geometry, Efficiency

**Corresponding authors. E-mail: Guiqiang.Li@hull.ac.uk (G. Li); Xudong.zhao@hull.ac.uk (X. Zhao);*

1. Introduction

Alternative energy conversion methods have received increased research attention because of environmental challenges such as; global warming, increasing energy demand and diminishing oil sources [1–3]. Asides the fact that these fossil fuel sources are limited, some other disadvantages include; creation of noise and exhaust gases, need for constant maintenance and repairs particularly for continuous operation [4,5]. Therefore, renewable energy sources like Photovoltaic (PV) technology offer unique advantages such as; noiseless operation, low maintenance and zero pollution [6]. The decrease of PV efficiency due to increasing cell temperature is the main shortcoming of the PV technology [7]. The best efficiency result obtained from a monocrystalline silicon cell is about 18% [8]. This value is quite low therefore, the efficiency of the PV cell needs to increase significantly to increase its comparative advantage over conventional energy sources and to encourage a wider adoption of the technology globally.

Photovoltaic cells utilize only part of the solar spectrum. Therefore, the infrared part of the sunlight which is not used by the PV cell heats up the cell and consequently, reduces the efficiency of the PV cell. Therefore, combining a PV cell which utilizes the visible and ultra-violet part of the sunlight with a Thermoelectric (TE) module which utilizes the infrared part of the sunlight would enable the utilization of the full solar spectrum [9]. The efficient combination of the PV and TE generators would constitute a significant breakthrough in solar energy utilization [10]. Research in the field of hybrid PV-TE has accelerated faster than other hybrid PV technologies [11]. A thermoelectric generator (TEG) is a solid state device which can convert heat directly into electricity by the Seebeck effect [12]. Therefore, the TEG attached to a PV performs a dual function of cooling the PV cell and generating extra electrical energy from the waste heat of the PV cell.

Research in the field of hybrid PV-TE has gained greater attention recently and different methods have been used to investigate the performance of the hybrid system. Van Sark [13] presented an idealized model for a hybrid PV-TE system and suggested that efficiency enhancement of about 50% could be achieved with the development of new TE materials. Ju et al. [14] presented a spectrum splitting hybrid PV-TE system using numerical modelling and observed that the cut-off wavelength of the hybrid system is mainly determined by the band gap of the solar cell. Park et al. [15] investigated a hybrid PV-TE system using a lossless coupling approach to improve the efficiency of the PV device in the hybrid system by 30%. Zhu et al. [16] used optimized thermal management techniques on a thermal concentrated hybrid PV-TE system which achieved peak efficiency of 23% during outdoor testing. Bjørk et al. [17] used an analytical model to determine the performance of hybrid PV-TE systems using different type of PV cells and found that the overall efficiency of the hybrid system can be lower than that of the PV only system. However, Lamba et al. [18] developed a theoretical model for analysing the performance of a concentrated PV-TEG and found that the hybrid system's power output and efficiency increased by 13.26% and 13.37% respectively in comparison with those of PV only system. Furthermore, Yin et al. [19] also developed a theoretical model for obtaining the one-day performance of a hybrid PV-TE system and observed a peak efficiency of 16.65%. In addition, Wu et al. [20] presented a theoretical model for determining the performance of glazed/unglazed hybrid PV-TE systems using nanofluid heat sink. The authors observed that nanofluid provides a better performance than water. Likewise, Soltani et al. [21] observed that nanofluid cooling enabled the highest power and efficiency improvements (54.29% and 3.35% respectively) in a hybrid PV-TE system in which five different cooling methods were investigated. To reduce the temperature fluctuations in a hybrid PV-TE system, Zhang et al. [22] developed a novel hybrid system in which the number of TE generator cooled by water could be adjusted by controlling the cycles of water in the cooling blocks. In addition to this, Cui et al. [23] introduced a phase change material (PCM) into a PV-TE system to mitigate temperature fluctuations in the system and observed improved performance. Furthermore, Mahmoudinezhad et al. [24] studied the transient response of a hybrid CPV-TE system and found that the thermal response of the TEG helps stabilize the temperature fluctuation in the hybrid system when solar radiation changes rapidly.

Finite Element Method (FEM) has been applied to the investigation of hybrid PV-TE system performance in the past. Kiflemariam et al. [25] used this method to perform a 2-D simulation of a hybrid PV-TE system and found that higher concentration ratio results in higher power production from the TEG module. Beeri et al. [26] also used this method along with experimental approach to investigate the performance of a PV-TE system and obtained a maximum efficiency of 32% for concentration ratio $\leq$ 200. More recently, Teffah et al. [27] used this method to investigate the efficiency of a hybrid system consisting of a triple junction solar cell (TJSC), a thermoelectric cooler (TEC) and a TEG. Furthermore, Li et al. [28] also used finite element method to optimise the geometry of the thermoelectric element footprint for maximum power generation in a PV-TE.

Recently, the incorporation of heat pipes into hybrid PV-TE systems have been investigated. Makki et al. [29] investigated a heat pipe based PV-TEG hybrid system and suggested that the system is better used in sunny regions with high operating temperature and low wind speeds. However, temperature independent material properties were used in the research. Furthermore, Li et al. [30] presented a novel PV-TE system based on a flat plate micro-channel heat pipe.

Considering the TEG geometry, Li et al. [31] studied the influence of geometric size on the performance of hybrid PV-TE systems and found that the overall efficiency increases as cross-sectional area increases. Furthermore, Hashim et al. [32] developed a model to determine the optimal geometry of thermoelectric devices in a hybrid PV-TE system. The authors argued that the dimension of the TEG in a hybrid system has a significant influence on the overall power output of the system. Li et al. [33] investigated the optimal geometry of the TEG element in a hybrid PV-TE uni-couple for maximum efficiency. The authors found that the hybrid system's maximum power output occurs when the ratio of area of n- and p-type (A_n/A_p) is symmetrical unlike in the case of a TEG only system. In addition, Kossyvakis et al. [34] advised the use of thermoelectric devices with shorter thermoelectric elements to obtain improved hybrid PV-TE system performance when operated under sufficient illumination. The authors suggested that this allow less material to be consumed and reduce system cost. These suggestions are in agreement with [35].

The optimized geometry of a TEG only system has been extensively studied in the past [36,37]. However, it is important to find the optimum geometry of the TEG when used in a hybrid PV-TE system. While previous works discussed above have considered the influence of the thermoelectric elements area ratio (A_n/A_p) on the efficiency of the hybrid system, to the best of our knowledge, there is no study on the influence of the cross sectional area ratio of each thermoelectric element (A_H/A_C) on the efficiency of the hybrid PV-TE system. A_n/A_p is the area ratio of the n-type and p-type thermoelectric elements while A_H/A_C is the area ratio of the thermoelectric element hot and cold junctions. In addition, some of the previous works have used constant thermoelectric material properties. However, the n- and p-type TE material properties are not the same in real applications and they also depend on temperature [33]. In fact, the power output and efficiency of a TEG is affected by the temperature dependency of the thermoelectric material properties [38]. Thus, it is imperative that temperature dependent thermoelectric material properties are used to avoid errors. Furthermore, temperature coefficient affects the efficiency of the PV only system [39].

However, there is limited research on its effect on the geometry and efficiency of the hybrid PV-TE system.

Therefore, this research investigates the optimum geometry for maximum efficiency in a hybrid PV-TE uni-couple. The advantage of using the uni-couple PV-TE model is that computational time can be significantly reduced while still achieving accurate results from which significant optimization activities can be carried out. In order to find this optimum geometry, the two thermoelectric element geometry area ratios are studied for the range $0.5 \leq R_A \leq 2$ and $0.5 \leq R_S \leq 2$. This range is used to investigate the performance of the hybrid PV-TE system because ease of fabrication of the thermoelectric element is considered. Presently, most thermoelectric elements are rectangular or square in shape and the rectangular shape corresponds to the condition $R_A = 1$ in this study. The other two conditions, $R_A = 0.5\ and\ 2$ modify the shape of the thermoelectric element into a trapezoidal shape which can also be fabricated. The goal is to simulate equivalent models which can be fabricated easily. The range $0.5 \leq R_S \leq 2$ controls the cross-sectional area of the thermoelectric elements (n-type and p-type). Also, the chosen range can be fabricated with ease therefore, it is used in the simulations.

In addition, the investigation is carried out at matched load condition and temperature dependent thermoelectric material properties are used. Nonlinearity of thermoelectric material properties used in modelling necessitates the use of computation techniques such as FEM software. The hybrid system is modelled in 3-dimension using COMSOL Multiphysics software and finite element method is used to solve the heat transfer equations. Finite Element Method (FEM) is used because of its Multiphysics simulation capability. Due to recent advancement in its Multiphysics simulation capability, the finite element method has become an attractive method to simulate thermoelectric devices. Furthermore, FEM allows Thomson effects and temperature dependent properties of thermoelectric materials to be easily coupled into the governing equations [40]. Some of the advantages of using finite element method are; it provides a user-friendly interface for model construction and results can be easily visualized. In addition, it provides increased simulation result accuracy [41]. The main advantage of this FEM software is that, it allows the coupling of different physical models. Also, it allows detailed investigation to be carried out to facilitate accurate design decision making because of its capability to allow optimization efforts to be carried out. Furthermore, the effect of PV temperature coefficient on the hybrid system maximum efficiency is studied for the three different geometric configurations considered.

The remaining part of this paper is organised as follows; Section 2 provides a detailed description of the different geometrical configurations used in the modelling and assumptions taken. Section 3 describes the mathematical model used and the modelling parameters utilized. Section 4 describes the results obtained and analysis of the results. Finally, the conclusions drawn from this study are presented in Section 5.

2. Geometry Description

The schematic diagrams of the different geometries of the hybrid system simulated are shown in Fig. 1, Fig. 2 and Fig. 3 corresponding to the range $0.5 \leq R_A \leq 2$ and $0.5 \leq R_S \leq 2$. The system consists of a solar concentrator, PV module, tedlar, and TEG module. The PV module is a Silicon cell and the TEG module consists of Bismuth Telluride thermoelectric elements which are connected electrically in series and thermally in parallel. Solar radiation passes through the solar concentrator and it is then impinged on the PV surface. Part of the solar radiation is converted to electricity directly by the PV module, some other part is lost to the environment by radiation and convection (thermal losses) while the remaining heat is transferred to the TEG module through heat conduction. The TEG hot side is attached to the bottom of the PV module and the TEG cold side is attached to a cooling base which is placed in ice water to take away the extra energy. Therefore, there is a temperature difference between the hot and cold sides of the TEG and electricity is generated by Seebeck effect. The following assumptions have been taken:

1. Only steady state conditions are considered.
2. The cold side of the TEG is maintained at a constant temperature of 273K.
3. Heat transfer occurs only in one dimension.
4. Two conversion efficiencies of PV (Cell A and Cell B) are considered (10% and 15%) for the two temperature coefficients used (0.001K^{-1} and 0.004K^{-1}) respectively and they change with temperature.

2.1 Geometric Configurations

The cross-sectional area of the different leg geometries of the thermoelectric generator in the hybrid system considered is shown in Fig. 4. Fig. 4a shows the leg geometry when $R_A = 0.5$, Fig. 4b shows the leg geometry when $R_A = 1$ and Fig. 4c shows the leg geometry when $R_A = 2$.

The nine different geometric configurations analysed are shown in Fig. 1, Fig. 2 and Fig. 3. The geometric configurations when $R_A = 0.5$ are shown in Fig. 1. For this case, Fig. 1a, Fig. 1b, Fig. 1c show the configurations when $R_S = 0.5$, $R_S = 1$ and $R_S = 2$ respectively. Furthermore, the geometric configurations when $R_A = 1$ are shown in Fig. 2. The configurations when $R_S = 0.5$, $R_S = 1$ and $R_S = 2$ are shown in Fig. 2a, Fig. 2b and Fig. 2c respectively for this case. Finally, Fig. 3 shows the geometric configurations when $R_A = 2$. For this case, Fig. 3a, Fig. 3b, Fig. 3c show the configurations when $R_S = 0.5$, $R_S = 1$ and $R_S = 2$ respectively.

3. Model Description

3.1 TEG Module

The mathematical equations corresponding to the leg geometries shown in Fig. 4 are [42]:

$$A(x) = \frac{A_H - A_C}{L} x + A_C \tag{1}$$

where A_C is the cross sectional area of the bottom side of the thermoelectric element and A_H is that of the top side. L is the height of the thermoelectric element. Therefore, the area ratio can be defined as $R_A = A_H/A_C$. The cross-sectional area of the thermoelectric element can be expressed as:

$$A(x) = A_0 \left[1 + 2\frac{R_A - 1}{R_A + 1}\left(\frac{x}{L} - \frac{1}{2}\right)\right] \tag{2}$$

where A_0 is the cross-sectional area of the uniform thermoelectric element.

The heat transfer rate through the leg along x is given by:

$$\dot{Q} = -kA(x)\frac{dT}{dx} \tag{3}$$

Assuming steady heating condition and isolated leg surfaces, equation (3) can be re-written as

$$\dot{Q}\int_0^L \frac{dx}{A(x)} = -k\int_{T_C}^{T_H} dT \tag{4}$$

Substituting equation (2) into equation (4) and performing integration

$$\dot{Q} = \frac{2k\frac{A_0}{L}\left(\frac{R_A - 1}{R_A + 1}\right)}{\ln(R_A)}(T_H - T_C) \tag{5}$$

The total thermal conductance of the thermoelectric generator considering the two legs shown in Fig. 1, Fig. 2 and Fig. 3 is given as

$$K = 2(k_p + k_n)\frac{\frac{A_0}{L}\left(\frac{R_A - 1}{R_A + 1}\right)}{\ln(R_A)} \tag{6}$$

where k_p and k_n are the thermal conductivities of the p-type and n-type legs respectively.

Also, considering the two legs the total electrical resistance of the thermoelectric generator is

$$R = \left(\frac{1}{\sigma_p} + \frac{1}{\sigma_n}\right)\frac{1}{2\frac{A_0}{L}\left(\frac{R_A-1}{R_A+1}\right)}\ln(R_A) = \frac{\sigma_p+\sigma_n}{2\sigma_p\sigma_n\frac{A_0}{L}\left(\frac{R_A-1}{R_A+1}\right)}\ln(R_A) \quad (7)$$

where σ_p and σ_n are the electrical conductivities of the p-type and n-type legs respectively.

Furthermore, R_S is the area ratio of the n-type and p-type thermoelectric element and can be expressed as: $R_S = A_n/A_p$.

where A_n is the cross-sectional area of the n-type thermoelectric element and A_p is the cross-sectional area of the p-type thermoelectric element.

3.2 PV Module

The following boundary conditions are applied to the PV module and are used to describe the FEM model.

External heat flux: This is applied at the upper surface of the PV cell and can be expressed as

$$q_0 = CG\alpha_{PV}A_{PV} - E_{PV}A_{PV} \quad (8)$$

The power output of the PV cell per square meter can be expressed as a function of solar irradiation and temperature as shown

$$E_{PV} = CGA_{PV}\eta_{PV}[1 - \varphi_c(T_{PV} - 298)] \quad (9)$$

Convective heat flux: This is considered at the upper surface of the PV cell due to the temperature difference between the upper surface and the ambient. It can be expressed as

$$q_1 = h_{amb}(T_{amb} - T_{PV}) \quad (10)$$

Diffuse surface: The heat transfer due to radiation at the surface of the PV cell can be expressed as

$$q_2 = \varepsilon\sigma_b(T_{amb}^4 - T_{PV}^4) \quad (11)$$

where σ_b is Stefan-Boltzmann's constant.

The last boundary condition is applied at the lower surface of the hybrid system. The cold side of the system is placed in ice water to maintain it at a constant temperature of 273K and this can be expressed as

$$T_C = T_0 = 273K \quad (12)$$

3.3 Overall System Performance

The performance of the hybrid PV-TE system is measured in terms of its overall electrical output and efficiency.

The total power output of the PV-TE system is the sum of the power outputs of PV and TEG and can be expressed as

$$P_{PV-TE} = P_{PV} + P_{TE} = E_{PV}A_{PV} + P_{TE} \quad (13)$$

The overall efficiency of the hybrid PV-TE system can be expressed as

$$\eta_{PV-TE} = \frac{P_{PV-TE}}{CGA_{PV}} = \frac{E_{PV}A_{PV}+P_{TE}}{CGA_{PV}} \quad (14)$$

3.4 Modelling Parameters

Different geometric parameters and material properties are used in modelling the hybrid PV-TE system. The Seebeck coefficient, Electrical conductivity and Thermal conductivity of the Bismuth Telluride (Bi_2Te_3) thermoelectric material used are temperature dependent and linearly extrapolated using the equations in Table 1 [43]. The remaining material properties used are listed in Table 2 while the geometric parameters used for modelling the hybrid PV-TE system are shown in Table 3.

The PV efficiency at standard test conditions is 10% for a PV cell with temperature coefficient of 0.001 K^{-1} (Cell A). While, the PV efficiency at standard test condition is 15% for a PV cell with temperature coefficient of 0.004 K^{-1} (Cell B).

4. Results and Discussion

The different geometrical configurations investigated are shown in Fig. 1, Fig. 2 and Fig. 3. COMSOL Multiphysics software is used to analyse the performance of each of these geometrical configurations. Different temperature and voltage distributions are obtained for each geometrical configuration as the load resistance (R_L) attached to the TEG is changed to find its optimum value for maximum hybrid system power output and efficiency. The optimum load resistance for a TEG only system is different from that of a TEG in a hybrid system [44]. The temperature and voltage distributions corresponding to the maximum efficiency obtained are shown in Fig. 5, Fig. 6 and Fig. 7 for $R_A = 0.5$, $R_A = 1$ and $R_A = 2$ respectively. These figures all correspond to the case when $R_S = 1$ and $\varphi_{PV} = 0.001/K$ (Cell A). Furthermore, temperature coefficient affects the temperature and voltage distributions in all the geometrical configurations investigated. Fig. 5a, Fig. 6a, and Fig. 7a show the temperature distributions for $R_A = 0.5$, $R_A = 1$ and $R_A = 2$ respectively. While Fig. 5b, Fig. 6b and Fig. 7b show the voltage distributions for $R_A = 0.5$, $R_A = 1$ and $R_A = 2$ respectively.

4.1 Geometry Area Ratios

The geometry of the thermoelectric elements in a hybrid PV-TE system influence the overall performance of the system which is measured in terms of its overall power output and conversion efficiency. Therefore, the two geometry area ratios which completely describe the geometry of thermoelectric elements in a hybrid PV-TE system are studied for the range to $0.5 \leq R_A \leq 2$ and $0.5 \leq R_S \leq 2$ and optimized to obtain the maximum efficiency from the hybrid system. In addition, the geometry area ratios are investigated for the two different PV temperature coefficient values considered and the results obtained are shown in Fig. 8 and Fig. 9.

It can be seen clearly from Fig. 8 and Fig. 9 that the maximum hybrid PV-TE system efficiency depends greatly on the geometry of the thermoelectric elements in the hybrid system. Furthermore, it can be seen that the temperature coefficient value plays an important role in determining the optimum geometry for the hybrid PV-TE system and consequently the maximum efficiency obtainable. The cross-sectional area ratio of the thermoelectric element hot and cold junctions ($R_A = A_H/A_C$) and the area ratio of the n-and p-type thermoelectric elements ($R_S = A_n/A_p$) are the two geometry area ratios analysed.

Fig. 8 shows that when $\varphi_{PV} = 0.001/K$ (Cell A), the optimum geometry for the thermoelectric element in the hybrid PV-TE system is dissymmetrical i.e. $R_A = R_S \neq 1$. In essence, the optimum geometry of the TEG in the hybrid system is the same as its geometry in a TEG only system because the temperature coefficient value of the PV is too low to affect its geometry in the hybrid system. Rezania et al. [45] and Al-Merbati et al. [42] found the optimum geometry of the thermoelectric elements in a TEG only system to be dissymmetrical. Furthermore, it can be seen that for all the values of R_S considered, the minimum efficiency all occur when $R_A = 1$. In addition, efficiency increase can be observed for $R_A = R_S = 0.5$ and $R_A = R_S = 2$ thus, implying that the optimum geometry of the thermoelectric element in a hybrid system to obtain the maximum overall efficiency is dissymmetrical. Although, the efficiency improvements might not be very significant now, the combination of several thermoelectric devices in series would lead to a more significant overall efficiency improvement.

Fig. 9 shows an opposite trend to results from Fig. 8 because the PV temperature coefficient has been increased to 0.004/K (Cell B). Furthermore, it is clear that the percentage increase in hybrid system efficiency values obtained for the different geometry area ratios in Fig. 9 is lower than those obtained in Fig. 8. This is because the efficiency of the hybrid PV-TE system decreases as the PV temperature coefficient increases [19]. In addition, the optimum geometry of the TEG in the hybrid system is symmetrical for this temperature coefficient value (0.004/K). Furthermore, it can be seen from Fig. 9 that the maximum efficiency occurs when $R_A = 1$ for all the values of R_S considered. Therefore, it can be concluded that when a high temperature coefficient value is used, the optimum geometry of the TEG in a hybrid system is different from its geometry in a TEG only system. This is a very important finding that will help researchers accurately choose the PV temperature coefficient value and geometrical configuration to be used for obtaining maximum efficiency.

4.2 Geometric Parameters

The thermoelectric element geometric parameters such as Height and Area can affect the maximum efficiency of the hybrid system. Furthermore, these geometric parameters also affect the temperature difference across the thermoelectric device and consequently, the power output from these devices. The effects of these geometric parameters on the overall hybrid system efficiency and TE temperature difference are shown in Fig. 10, Fig. 11, Fig. 12, Fig. 13, Fig. 14 and Fig. 15 for $0.5 \leq R_A \leq 2$, $R_S = 1$, $\varphi_{PV} = 0.001/K$ (Cell A) and $\varphi_{PV} = 0.004/K$ (Cell B).

4.2.1 Case A ($R_A = 0.5$)

It can be seen from Fig. 10a and Fig. 10b that the overall efficiency of the hybrid system shows a decreasing trend as the thermoelectric element height increases. In addition, it is clear that the PV temperature coefficient value affects the steepness of the efficiency deep as thermoelectric element height increases. Therefore, shorter thermoelectric elements should be used to obtain improved hybrid PV-TE efficiency. Furthermore, it can be seen from both Fig. 10a and Fig. 10b that the overall efficiency of the hybrid system increases as the cross-sectional area of the thermoelectric element increases. This is true no matter the temperature coefficient value used thus, there is an optimum thermoelectric element height and area which gives the maximum hybrid system efficiency. In addition, it can be seen from Fig. 10b that the efficiency of the hybrid system for some thermoelectric element height and area is lower in comparison with the standard efficiency of the PV cell (15%). This can also be observed from Fig. 10a where the standard efficiency of the PV cell (10%) is greater than that of the hybrid system for some thermoelectric element height and area. This implies that it is very important to find the optimum geometry for the thermoelectric element in the hybrid PV-TE system if high overall efficiency is desired.

Fig. 11 shows the variation of the TE temperature difference with thermoelectric element area and height. It can be seen that the temperature difference decreases as the thermoelectric element area increases. This is the result for both temperature coefficient values considered. Furthermore, it can be seen that the temperature difference increases as the thermoelectric element height increases and area increases however, it gets saturated at some point and the increase is no longer significant. Therefore, determining the optimum geometry of the thermoelectric elements in the hybrid PV-TE system would help reduce the amount of material consumed and reduce system cost.

4.2.2 Case B ($R_A = 1$)

Fig. 12 shows the variation of overall system efficiency with thermoelectric element height and area. It can be seen from Fig. 12b that the hybrid system efficiency shows a decreasing trend as the thermoelectric element height increases and an increasing trend as the thermoelectric element area increases when $\varphi_{PV} = 0.004/K$. However, Fig. 12a shows that when $\varphi_{PV} = 0.001/K$, the overall efficiency initially increases before decreasing as the thermoelectric element height increases for some certain thermoelectric element area. This implies that maximum hybrid system efficiency can be obtained using some specific geometry parameters.

As observed in Fig. 11, Fig. 13 shows a similar TE temperature difference decreasing trend as TE area increases. This is the result for both temperature coefficient values considered.

4.2.3 Case C ($R_A = 2$)

The variation of overall hybrid system efficient with thermoelectric element height and area is shown in Fig. 14a and Fig. 14b for both temperature coefficient values considered respectively. Furthermore, the variation of TE temperature difference with TE area for $\varphi_{PV} = 0.001/K$ and $\varphi_{PV} = 0.004/K$ have the same trend and values and is shown in Fig. 15. In addition, it can be seen from Fig. 14a that the overall efficiency values obtained for this Case C are slightly higher than those obtained for Case A (Fig. 10a). Therefore, the optimum geometry for a thermoelectric element in a hybrid PV-TE system when $\varphi_{PV} = 0.001/K$ is $R_A = 2$. However, the optimum geometry when $\varphi_{PV} = 0.004/K$ is $R_A = 1$.

4.3 Irradiation

The solar irradiance value and concentration ratio determine the amount of heat flux at the surface of the PV cell and consequently, the performance of the hybrid PV-TE system. The effect of solar irradiance and concentration ratio on the performance of the hybrid system is investigated when $A_{TE} = 14mm^2$, $L_{TE} = 5mm$, $R_A = R_S = 1$ and $\varphi_{PV} = 0.004/K$ (Cell B). These conditions are chosen because they provide the optimum hybrid system performance based on the findings presented earlier. The hybrid photovoltaic-thermoelectric system will operate in an optimized state using these conditions because maximum efficiency will be obtained.

Fig. 16 shows the variation of PV-TE efficiency with solar irradiance for the temperature coefficient value considered. It can be seen that the hybrid system efficiency shows a decreasing trend as solar irradiance increases. This is because the PV module temperature increases with increase in solar irradiance and this affects the overall efficiency of the hybrid system. Therefore, the efficiency curve of the hybrid PV-TE system will follow the same trend as that of the PV system.

Fig. 17a and Fig. 17b show the variation of PV and TEG power outputs with solar irradiance at different concentration ratio respectively. It can be seen clearly that PV power output increases linearly with solar irradiance for all the concentration ratio considered. The same is not completely the case with the TEG power output although it also increases as solar irradiance and concentration ratio increase. It can also be concluded that high power outputs can be obtained from both the PV and TEG when high values of solar irradiance and concentration ratio are used. The power output of the TEG increases as solar irradiance increases due to the increase in the module temperature which leads to higher temperature difference across the module as shown in Fig. 17b. In addition, it can also be seen from Fig.

17b that the TEG power output increases with an increase in concentration ratio and this is due to an increased heat flux supplied to the TEG module.

The variation of power outputs from the PV, TEG and PV-TE systems with concentration ratio when $G = 1000\ W/m^2$ is shown in Fig. 18. It is obvious that the PV provides the greater percentage of the total hybrid system power output. The contribution of the TEG is very small compared to that of the PV in terms of power output however, the TE also helps to cool the PV thus, increasing the life-span of the PV system. When more thermoelectric modules are used, the power output from the TEG would be much greater than those shown in Fig. 18 because only a uni-couple is investigated in this research.

The variation of temperature of PV system with solar irradiance at different concentration ratio is shown in Fig. 19. It can be seen clearly that the temperature at the surface of the PV cell varies linearly with solar irradiance for all the concentration ratio investigated. It is generally known that high temperature in the PV system results in low efficiency thus, it is important to carefully consider which solar irradiance value and concentration ratio would be used. Furthermore, Fig. 16b shows that low concentration ratio could produce the highest efficiency when $\varphi_{PV} = 0.004/K$ and this is due to the low PV temperatures corresponding to such low concentration ratio which is shown in Fig. 19.

5. Conclusion

The optimum geometry of a thermoelectric element in a hybrid PV-TE system has been investigated in this research using finite element method. The 3-D numerical model for the different thermoelectric element geometries investigated was built for the hybrid PV-TE system and it was accurately meshed into small tetrahedrons to increase the accuracy of the results obtained. COMSOL Multiphysics was used to solve the FEM equations and determine the optimum geometry for the thermoelectric element in a hybrid PV-TE system. Two geometry area ratios which completely describe the geometry of the thermoelectric element was investigated for the range $0.5 \leq R_A \leq 2$ and $0.5 \leq R_S \leq 2$. Ra is the cross-sectional area ratio of the thermoelectric element hot and cold junctions (A_H/A_C) while Rs is the area ratio of the n- and p-type thermoelectric elements (A_n/A_p).

Nine different geometric configurations were analysed for two different PV cells. Temperature dependent TE material properties were used to ensure accurate results were obtained. The temperature and voltage distributions in the hybrid system for the different geometric configurations considered were presented. The results obtained show that the PV temperature coefficient value affects the geometry and efficiency of the hybrid system. It was found that the hybrid PV-TE system performs better with symmetrical TEG geometry ($R_A = R_S = 1$) if a PV temperature coefficient of 0.004/K (Cell B) is used. This is different from the optimum geometry for a TEG only system. However, the optimum geometry of the TEG in a hybrid system will be the same as that of a TEG only system (dissymmetrical i.e. $R_A = R_S \neq 1$) if a PV temperature coefficient of 0.001/K (Cell A) is used.

Geometric parameters such as thermoelectric element height and area were found to influence the performance of the hybrid PV-TE system. In general, thermoelectric element with shorter heights and higher cross sectional area should be used to obtain maximum hybrid system efficiency. One constant thing observed was that overall efficiency and TE temperature difference show a decreasing trend as thermoelectric element length and area increases for all the geometric configuration and temperature coefficient values considered.

The effects of solar irradiation and concentration ratio on the performance of the hybrid system were also analysed. It was found that low concentration ratio produce high overall hybrid system efficiency when $\varphi_{PV} = 0.004/K$ and this is due to the low PV temperatures corresponding to such low concentration ratio. Furthermore, it was found that the PV provides the greater percentage of the total hybrid system power output. The contribution of the TEG was very small compared to that of the PV in terms of power output. In addition, it can be concluded that high power outputs can be obtained from both the PV and TEG when high values of solar irradiance and concentration ratio are used. In summary, it was found that the hybrid system efficiency showed a decreasing trend as solar irradiance increased when $\varphi_{PV} = 0.004/K$.

Acknowledgment

This study was sponsored by the Project of EU Marie Curie International Incoming Fellowships Program (745614).The authors would also like to express our appreciation for the financial supports from EPSRC (EP/R004684/1) and Innovate-UK (TSB 70507-481546) for the Newton Fund – China-UK Research and Innovation Bridges Competition 2015 Project 'A High Efficiency, Low Cost and Building Integrate-able Solar Photovoltaic/Thermal (PV/T) System for Space Heating, Hot Water and Power Supply' and DongGuan Innovative Research Team Program (No. 2014607101008).

References

[1] U. Erturun, K. Erermis, K. Mossi, Effect of various leg geometries on thermo-mechanical and power generation performance of thermoelectric devices, Appl. Therm. Eng. 73 (2014) 126–139. doi:10.1016/j.applthermaleng.2014.07.027.

[2] G. Li, S. Shittu, T.M.O. Diallo, M. Yu, X. Zhao, J. Ji, A review of solar photovoltaic-thermoelectric hybrid system for electricity generation, Energy. 158 (2018) 41–58. doi:https://doi.org/10.1016/j.energy.2018.06.021.

[3] Z. Liu, D. Wu, H. Yu, W. Ma, G. Jin, Field measurement and numerical simulation of

combined solar heating operation modes for domestic buildings based on the Qinghai–Tibetan plateau case, Energy Build. 167 (2018) 312–321. doi:https://doi.org/10.1016/j.enbuild.2018.03.016.

[4] R. Kugele, W. Roth, W. Schulz, A. Steinhuser, Thermoelectric generators in photovoltaic hybrid systems, in: 15th Int. Conf. Thermoelectr. Proc. ICT ’96, 26-29 March 1996, 1996: pp. 352–356. doi:10.1109/ICT.1996.553505.

[5] A. Steinhiiser, G. Hille, R. Kiigele, W. Roth, W. Schulz, Reliable Power Supply With Photovoltaic-Thermoelectric Hybrid Systems, in: Telescon ’97 - Second Int. Telecommun. Energy Spec. Conf. Budapest, Hungary, April 21-25, 1997: pp. 111–117.

[6] C. Ramulu, T. Praveen Kumar, S. Jain, Single stage PV source based dual inverter fed open-end winding induction motor pump drive, in: 2014 IEEE Students’ Conf. Electr. Electron. Comput. Sci. SCEECS 2014, 2014: pp. 0–5. doi:10.1109/SCEECS.2014.6804459.

[7] D. Narducci, B. Lorenzi, Challenges and perspectives in tandem thermoelectric-photovoltaic solar energy conversion, IEEE Trans. Nanotechnol. 15 (2016) 348–355. doi:10.1109/TNANO.2016.2524680.

[8] M. Fisac, F.X. Villasevil, A.M. López, High-efficiency photovoltaic technology including thermoelectric generation, J. Power Sources. 252 (2014) 264–269. doi:10.1016/j.jpowsour.2013.11.121.

[9] E. Elsarrag, H. Pernau, J. Heuer, N. Roshan, Y. Alhorr, K. Bartholomé, Spectrum splitting for efficient utilization of solar radiation: a novel photovoltaic–thermoelectric power generation system, Renewables Wind. Water, Sol. 2 (2015) 16. doi:10.1186/s40807-015-0016-y.

[10] P. Huen, W.A. Daoud, Advances in hybrid solar photovoltaic and thermoelectric

generators, Renew. Sustain. Energy Rev. 72 (2017) 1295–1302. doi:10.1016/j.rser.2016.10.042.

[11] C. Babu, P. Ponnambalam, The role of thermoelectric generators in the hybrid PV/T systems: A review, Energy Convers. Manag. 151 (2017) 368–385. doi:10.1016/j.enconman.2017.08.060.

[12] N. Wang, L. Han, H. He, N. Park, K. Koumoto, A novel high-performance photovoltaic-thermoelectric hybrid device, Energy Environ. Sci. 4 (2011) 3676–3679. doi:10.1039/c1ee01646f.

[13] W.G.J.H.M. Van Sark, Feasibility of photovoltaic - Thermoelectric hybrid modules, Appl. Energy. 88 (2011) 2785–2790. doi:10.1016/j.apenergy.2011.02.008.

[14] X. Ju, Z. Wang, G. Flamant, P. Li, W. Zhao, Numerical analysis and optimization of a spectrum splitting concentration photovoltaic-thermoelectric hybrid system, Sol. Energy. 86 (2012) 1941–1954. doi:10.1016/j.solener.2012.02.024.

[15] K.T. Park, S.M. Shin, A.S. Tazebay, H.D. Um, J.Y. Jung, S.W. Jee, M.W. Oh, S.D. Park, B. Yoo, C. Yu, J.H. Lee, Lossless hybridization between photovoltaic and thermoelectric devices, Sci. Rep. 3 (2013) 1–6. doi:10.1038/srep02123.

[16] W. Zhu, Y. Deng, Y. Wang, S. Shen, R. Gulfam, High-performance photovoltaic-thermoelectric hybrid power generation system with optimized thermal management, Energy. 100 (2016) 91–101. doi:10.1016/j.energy.2016.01.055.

[17] R. Bjørk, K.K. Nielsen, The performance of a combined solar photovoltaic (PV) and thermoelectric generator (TEG) system, Sol. Energy. 120 (2015) 187–194. doi:10.1016/j.solener.2015.07.035.

[18] R. Lamba, S.C. Kaushik, Modeling and performance analysis of a concentrated photovoltaic-thermoelectric hybrid power generation system, Energy Convers. Manag. 115 (2016) 288–298. doi:10.1016/j.enconman.2016.02.061.

[19] E. Yin, Q. Li, Y. Xuan, One-day performance evaluation of photovoltaic-thermoelectric hybrid system, Energy. 143 (2018) 337–346. doi:10.1016/j.energy.2017.11.011.

[20] Y.Y. Wu, S.Y. Wu, L. Xiao, Performance analysis of photovoltaic-thermoelectric hybrid system with and without glass cover, Energy Convers. Manag. 93 (2015) 151–159. doi:10.1016/j.enconman.2015.01.013.

[21] S. Soltani, A. Kasaeian, H. Sarrafha, D. Wen, An experimental investigation of a hybrid photovoltaic/thermoelectric system with nanofluid application, Sol. Energy. 155 (2017) 1033–1043. doi:10.1016/j.solener.2017.06.069.

[22] J. Zhang, Y. Xuan, Performance improvement of a photovoltaic - Thermoelectric hybrid system subjecting to fluctuant solar radiation, Renew. Energy. 113 (2017) 1551–1558. doi:10.1016/j.renene.2017.07.003.

[23] T. Cui, Y. Xuan, Q. Li, Design of a novel concentrating photovoltaic-thermoelectric system incorporated with phase change materials, Energy Convers. Manag. 112 (2016) 49–60. doi:10.1016/j.enconman.2016.01.008.

[24] S. Mahmoudinezhad, A. Rezania, L.A. Rosendahl, Behavior of hybrid concentrated photovoltaic-thermoelectric generator under variable solar radiation, Energy Convers. Manag. 164 (2018) 443–452. doi:10.1016/j.enconman.2018.03.025.

[25] R. Kiflemariam, M. Almas, C. Lin, Modeling Integrated Thermoelectric Generator-Photovoltaic Thermal (TEG-PVT) System, Proc. 2014 COMSOL Conf. (2014) 1–5. doi:10.1016/j.rser.2005.06.008.

[26] O. Beeri, O. Rotem, E. Hazan, E.A. Katz, A. Braun, Hybrid photovoltaic-thermoelectric system for concentrated solar energy conversion : Experimental realization and modeling, J. Appl. Phys. 118 (2015) 115104. doi:10.1063/1.4931428.

[27] K. Teffah, Y. Zhang, Modeling and experimental research of hybrid PV-thermoelectric

system for high concentrated solar energy conversion, Sol. Energy. 157 (2017) 10–19. doi:10.1016/j.solener.2017.08.017.

[28] G. Li, X. Zhao, Y. Jin, X. Chen, J. Ji, S. Shittu, Performance Analysis and Discussion on the Thermoelectric Element Footprint for PV–TE Maximum Power Generation, J. Electron. Mater. (2018). doi:https://doi.org/10.1007/s11664-018-6421-4.

[29] A. Makki, S. Omer, Y. Su, H. Sabir, Numerical investigation of heat pipe-based photovoltaic-thermoelectric generator (HP-PV/TEG) hybrid system, Energy Convers. Manag. 112 (2016) 274–287. doi:10.1016/j.enconman.2015.12.069.

[30] G. Li, X. Zhao, J. Ji, Conceptual development of a novel photovoltaic-thermoelectric system and preliminary economic analysis, Energy Convers. Manag. 126 (2016) 935–943. doi:10.1016/j.enconman.2016.08.074.

[31] G. Li, X. Chen, Y. Jin, Analysis of the primary constraint conditions of an efficient photovoltaic-thermoelectric hybrid system, Energies. 10 (2017) 1–12. doi:10.3390/en10010020.

[32] H. Hashim, J.J. Bomphrey, G. Min, Model for geometry optimisation of thermoelectric devices in a hybrid PV/TE system, Renew. Energy. 87 (2016) 458–463. doi:10.1016/j.renene.2015.10.029.

[33] G. Li, X. Chen, Y. Jin, J. Ji, Optimizing on thermoelectric elements footprint of the photovoltaic-thermoelectric for maximum power generation, Energy Procedia. 142 (2017) 730–735. doi:10.1016/j.egypro.2017.12.119.

[34] D.N. Kossyvakis, G.D. Voutsinas, E. V. Hristoforou, Experimental analysis and performance evaluation of a tandem photovoltaic-thermoelectric hybrid system, Energy Convers. Manag. 117 (2016) 490–500. doi:10.1016/j.enconman.2016.03.023.

[35] D. Kraemer, K. McEnaney, M. Chiesa, G. Chen, Modeling and optimization of solar thermoelectric generators for terrestrial applications, Sol. Energy. 86 (2012) 1338–

1350. doi:10.1016/j.solener.2012.01.025.

[36] W.H. Chen, C.C. Wang, C.I. Hung, C.C. Yang, R.C. Juang, Modeling and simulation for the design of thermal-concentrated solar thermoelectric generator, Energy. 64 (2014) 287–297. doi:10.1016/j.energy.2013.10.073.

[37] Z. Liu, S. Zhu, Y. Ge, F. Shan, L. Zeng, W. Liu, Geometry optimization of two-stage thermoelectric generators using simplified conjugate-gradient method, Appl. Energy. 190 (2017) 540–552. doi:10.1016/j.apenergy.2017.01.002.

[38] F. Meng, L. Chen, F. Sun, Effects of temperature dependence of thermoelectric properties on the power and efficiency of a multielement thermoelectric generator, Int. J. Energy Environ. 3 (2012) 137–150.

[39] E. Skoplaki, J.A. Palyvos, On the temperature dependence of photovoltaic module electrical performance: A review of efficiency/power correlations, Sol. Energy. 83 (2009) 614–624. doi:10.1016/j.solener.2008.10.008.

[40] G. Wu, X. Yu, A holistic 3D finite element simulation model for thermoelectric power generator element, Energy Convers. Manag. 86 (2014) 99–110. doi:10.1016/j.enconman.2014.04.040.

[41] G. Fraisse, J. Ramousse, D. Sgorlon, C. Goupil, Comparison of different modeling approaches for thermoelectric elements, Energy Convers. Manag. 65 (2013) 351–356. doi:10.1016/j.enconman.2012.08.022.

[42] A.S. Al-Merbati, B.S. Yilbas, A.Z. Sahin, Thermodynamics and thermal stress analysis of thermoelectric power generator: Influence of pin geometry on device performance, Appl. Therm. Eng. 50 (2013) 683–692. doi:10.1016/j.applthermaleng.2012.07.021.

[43] R.O. Suzuki, K.O. Ito, S. Oki, Analysis of the Performance of Thermoelectric Modules Under Concentrated Radiation Heat Flux, J. Electron. Mater. 45 (2016) 1827–1835. doi:10.1007/s11664-015-4237-z.

[44] G. Li, K. Zhou, Z. Song, X. Zhao, J. Ji, Inconsistent phenomenon of thermoelectric load resistance for photovoltaic–thermoelectric module, Energy Convers. Manag. 161 (2018) 155–161. doi:10.1016/j.enconman.2018.01.079.

[45] A. Rezania, L.A. Rosendahl, H. Yin, Parametric optimization of thermoelectric elements footprint for maximum power generation, J. Power Sources. 255 (2014) 151–156. doi:10.1016/j.jpowsour.2014.01.002.

[46] G. Li, G. Pei, J. Ji, Y. Su, Outdoor overall performance of a novel air-gap-lens-walled compound parabolic concentrator (ALCPC) incorporated with photovoltaic/thermal system, Appl. Energy. 144 (2015) 214–223. doi:10.1016/j.apenergy.2015.01.112.

Nomenclature

A	Area, m^2	***Greek Symbols***	
C	Concentration ratio	α	Absorptivity
C_P	Specific heat capacity, $J/(kg \cdot K)$	φ	PV temperature coefficient, K^{-1}
E_{PV}	Power output of PV per square meter, W/m^2	η	Efficiency
G	Solar irradiance, W/m^2	η_{ref}	Efficiency of PV cell under standard test conditions
h_{amb}	Convective heat transfer coefficient on outer surface, $W/(m^2 \cdot K)$	ε	Emissivity
k	Thermal conductivity, $W/(m \cdot K)$	σ	Electrical conductivity, S/m

L	Height, m	ρ	Density, kgm^{-3}
P	Power output, W	***Subscripts***	
q_0	Heat flux, W/m^2	amb	Ambient
R_A	Cross-sectional area ratio of TE hot and cold junctions	C	Cold side
R_L	Load resistance on TEG, Ω	H	Hot side
R_S	Area ratio of n- and p-type TE modules	n	n-type
S	Seebeck coefficient of TE module, V/K	p	p-type
T	Temperature, K	***Abbreviations***	
ΔT	Temperature difference, K $\Delta T = T_H - T_C$	PV	Photovoltaic
u_w	Wind velocity, m/s	TE	Thermoelectric

Figure captions

Fig. 1. Schematic diagrams of a PV-TE with different leg geometries for $R_A = 0.5$ and a) $R_S = 0.5$ b) $R_S = 1$ c) $R_S = 2$.

Fig. 2. Schematic diagrams of a PV-TE with different leg geometries for $R_A = 1$ and a) $R_S = 0.5$ b) $R_S = 1$ c) $R_S = 2$.

Fig. 3. Schematic diagrams of a PV-TE with different leg geometries for $R_A = 2$ and a) $R_S = 0.5$ b) $R_S = 1$ c) $R_S = 2$.

Fig. 4. Different leg geometric configurations for a) $R_A = 0.5$ b) $R_A = 1$ c) $R_A = 2$.

Fig. 5. PV-TE 3-dimensional a) Temperature and b) Voltage distributions for $R_A = 0.5$.

Fig. 6. PV-TE 3-dimensional a) Temperature and b) Voltage distributions for $R_A = 1$.

Fig. 7. PV-TE 3-dimensional a) Temperature and b) Voltage distributions for $R_A = 2$.

Fig. 8. Overall PV-TE efficiency vs geometry area ratios for Cell A.

Fig. 9. Overall PV-TE efficiency vs geometry area ratios for Cell B.

Fig. 10. Hybrid system efficiency vs thermoelectric element height for $R_A = 0.5$ and a) Cell A b) Cell B.

Fig. 11. Thermoelectric temperature difference vs thermoelectric area for $R_A = 0.5$ and both PV cells (Cell A and Cell B).

Fig. 12. Hybrid system efficiency vs thermoelectric element height for $R_A = 1$ and a) Cell A b) Cell B.

Fig. 13. Thermoelectric temperature difference vs thermoelectric area for $R_A = 1$ and both PV cells (Cell A and Cell B).

Fig. 14. Hybrid system efficiency vs thermoelectric element height for $R_A = 2$ and a) Cell A b) Cell B.

Fig. 15. Thermoelectric temperature difference vs thermoelectric area for $R_A = 2$ and both PV cells (Cell A and Cell B).

Fig. 16. Hybrid system efficiency vs solar irradiance and concentration ratio.

Fig. 17. Variation of a) PV and b) TEG power outputs with solar irradiance and concentration ratio.

Fig. 18. Variation of PV, TEG and PV-TE power outputs with concentration ratio.

Fig. 19. Variation of PV surface temperature with solar irradiance and concentration ratio for Cell B.

Table list

Table 1. Temperature dependent material properties (T is temperature in K) [43].

Table 2. Material properties [18,20,27].

Table 3. Parameters used in hybrid PV-TE model.

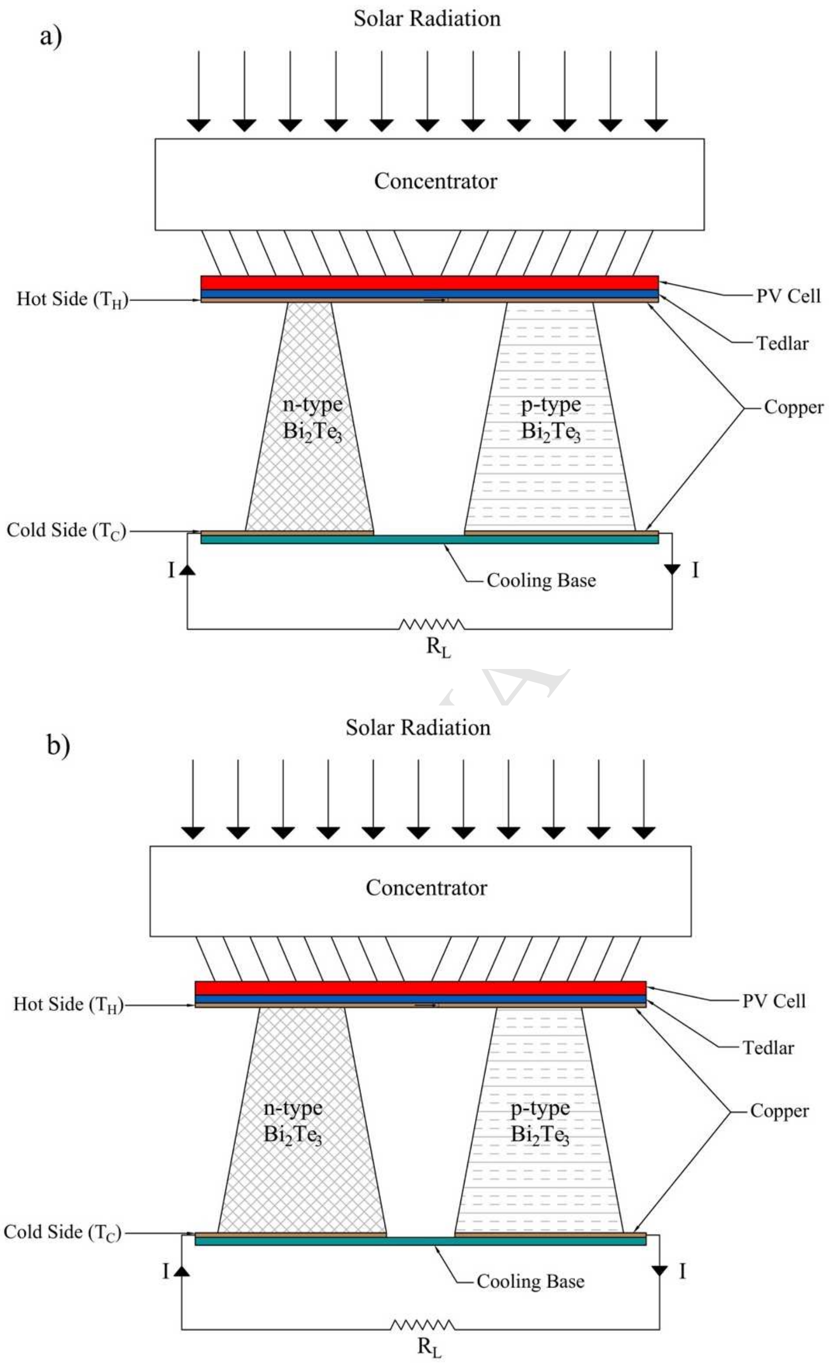
a)
Solar Radiation
Concentrator
Hot Side (T_H)
PV Cell
Tedlar
Copper
n-type
Bi_2Te_3
p-type
Bi_2Te_3
Cold Side (T_C)
I
Cooling Base
I
R_L
b)
Solar Radiation
Concentrator
Hot Side (T_H)
PV Cell
Tedlar
Copper
n-type
Bi_2Te_3
p-type
Bi_2Te_3
Cold Side (T_C)
I
Cooling Base
I
R_L

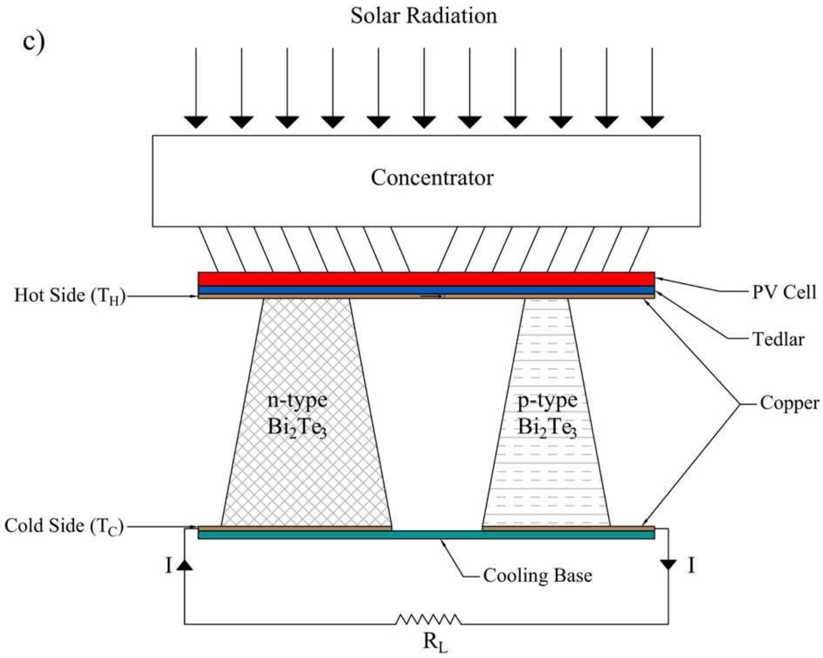

Fig. 1. Schematic diagrams of a PV-TE with different leg geometries for $R_A = 0.5$ and a) $R_S = 0.5$ b) $R_S = 1$ c) $R_S = 2$.

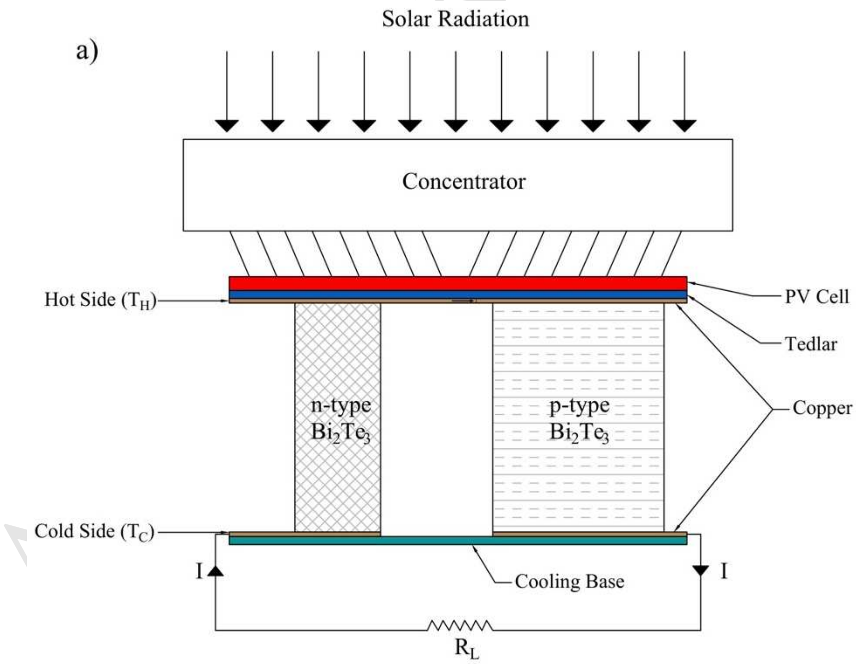

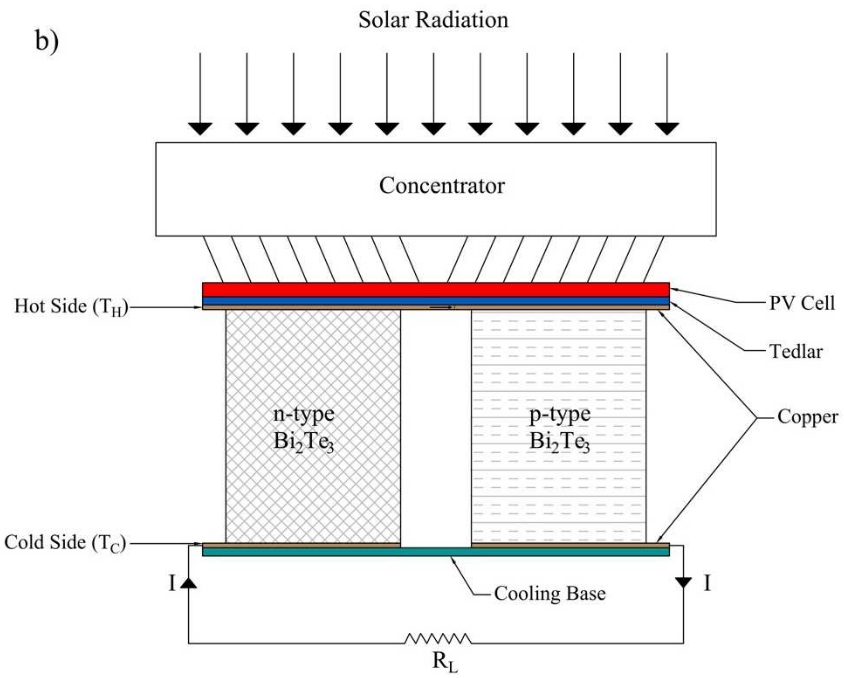

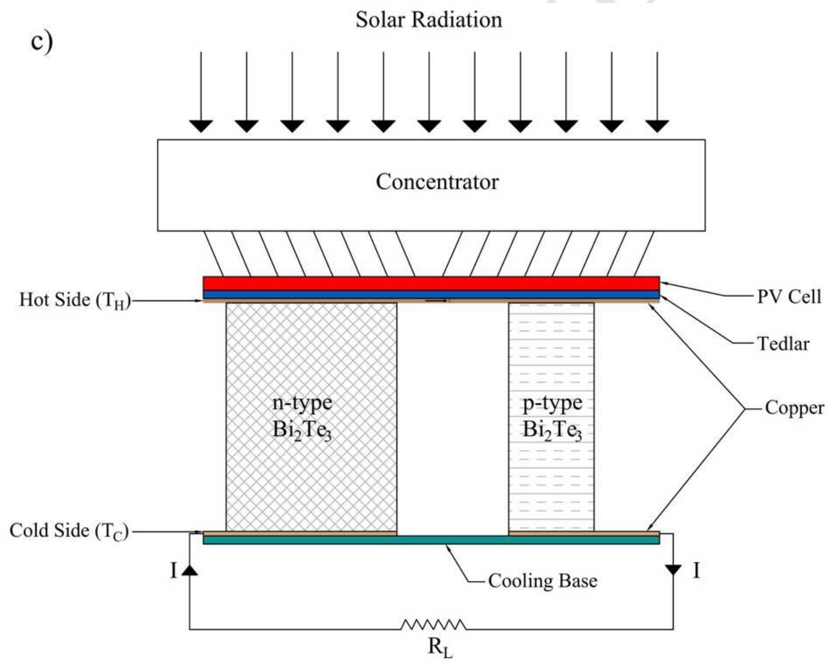

Fig. 2. Schematic diagrams of a PV-TE with different leg geometries for $R_A = 1$ and a) $R_S = 0.5$ b) $R_S = 1$ c) $R_S = 2$.

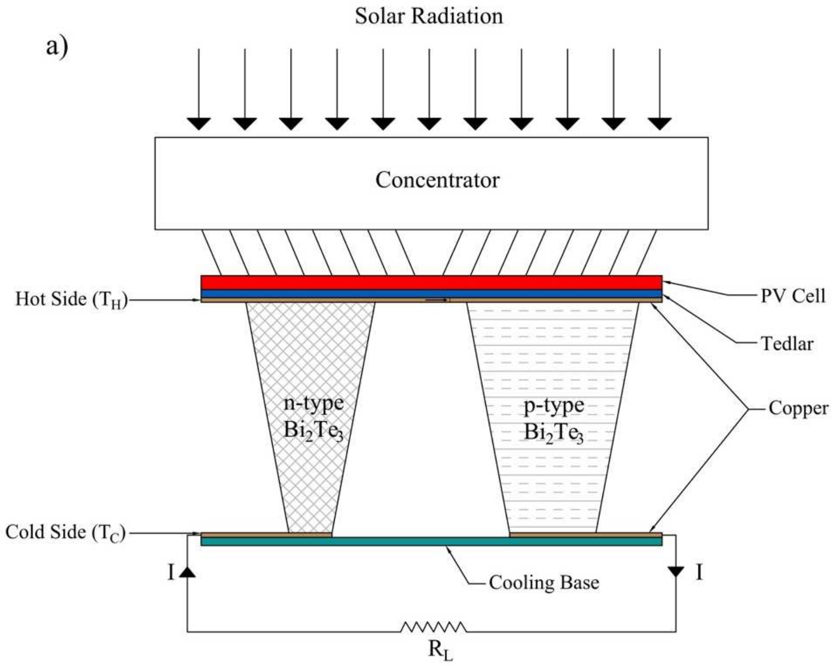
Solar Radiation
a)
Concentrator
Hot Side (T_H)
PV Cell
Tedlar
Copper
n-type
Bi2Te3
p-type
Bi2Te3
Cold Side (T_C)
I
Cooling Base
I
R_L

725

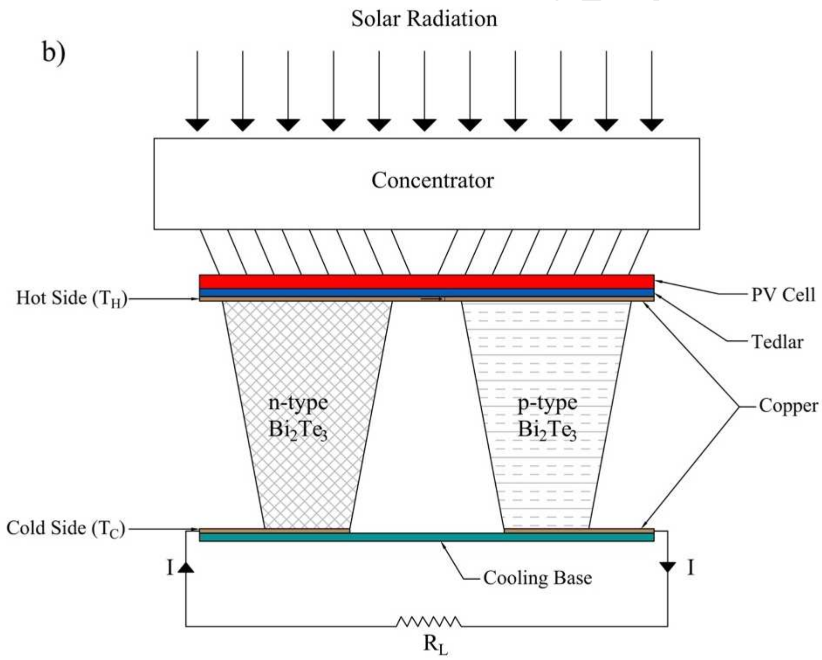
Solar Radiation
b)
Concentrator
Hot Side (T_H)
PV Cell
Tedlar
Copper
n-type
Bi2Te3
p-type
Bi2Te3
Cold Side (T_C)
I
Cooling Base
I
R_L

726

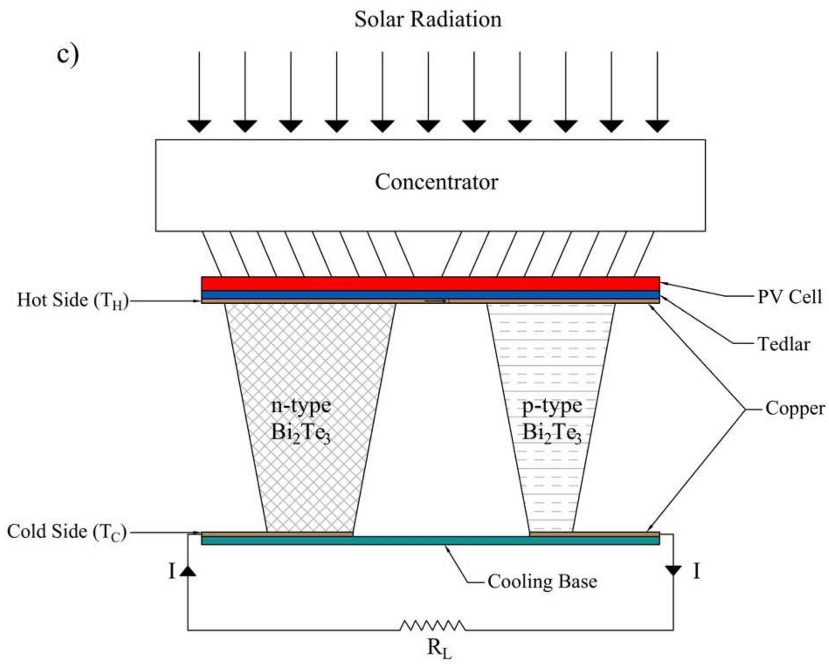

Fig. 3. Schematic diagrams of a PV-TE with different leg geometries for $R_A = 2$ and a) $R_S = 0.5$ b) $R_S = 1$ c) $R_S = 2$.

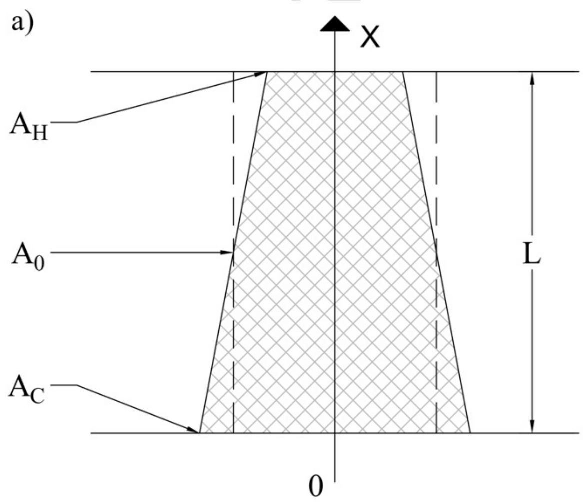

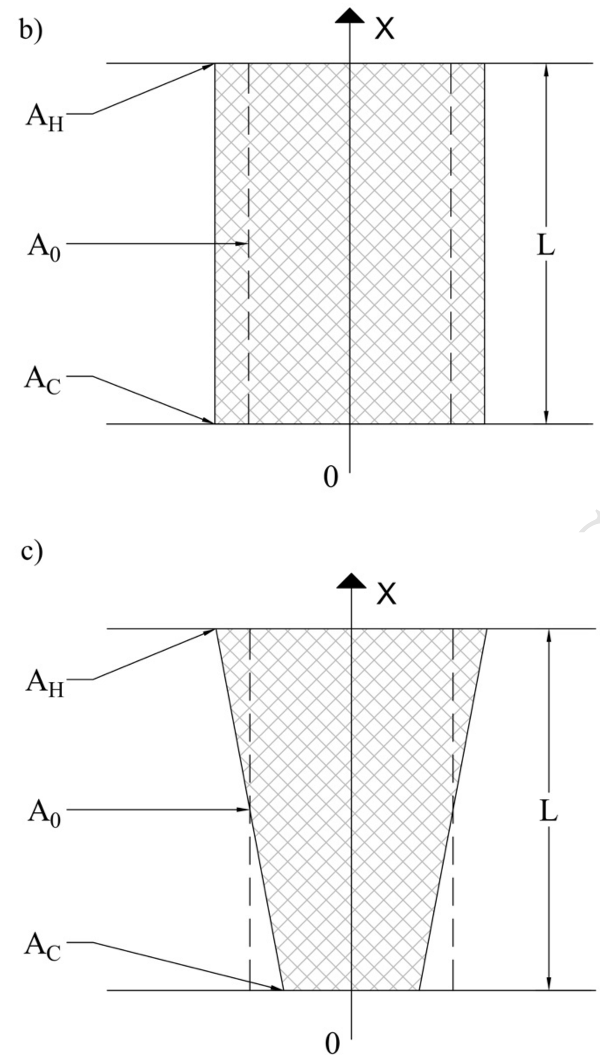

Fig. 4. Different leg geometric configurations for a) $R_A = 0.5$ b) $R_A = 1$ c) $R_A = 2$.

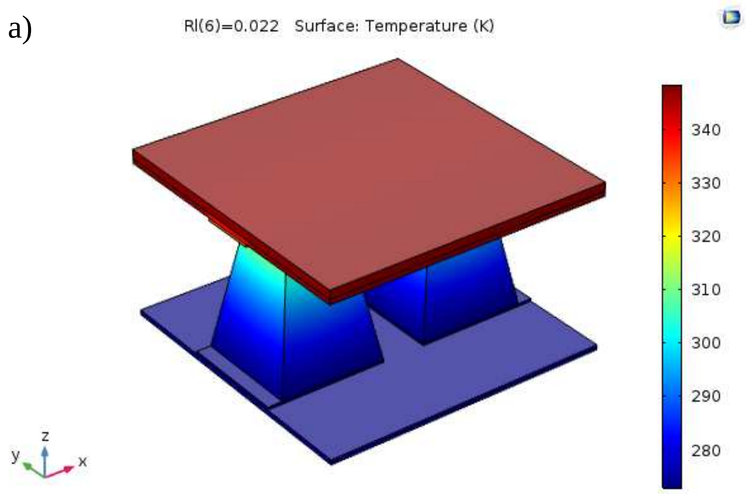

b)

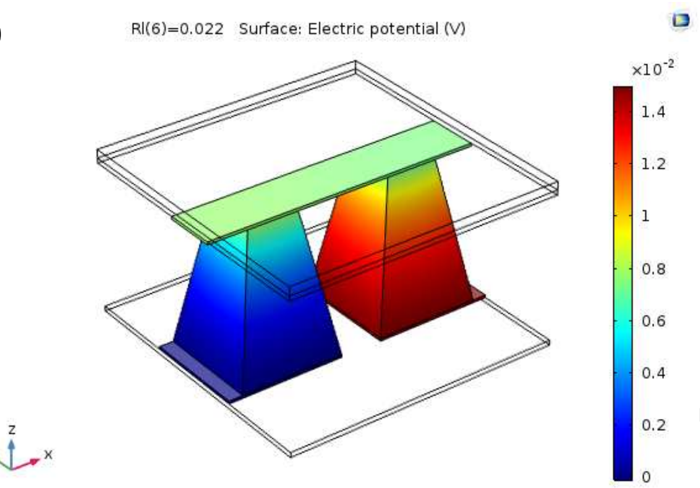

Fig. 5. PV-TE 3-dimensional a) Temperature and b) Voltage distributions for $R_A = 0.5$.

a)

b)

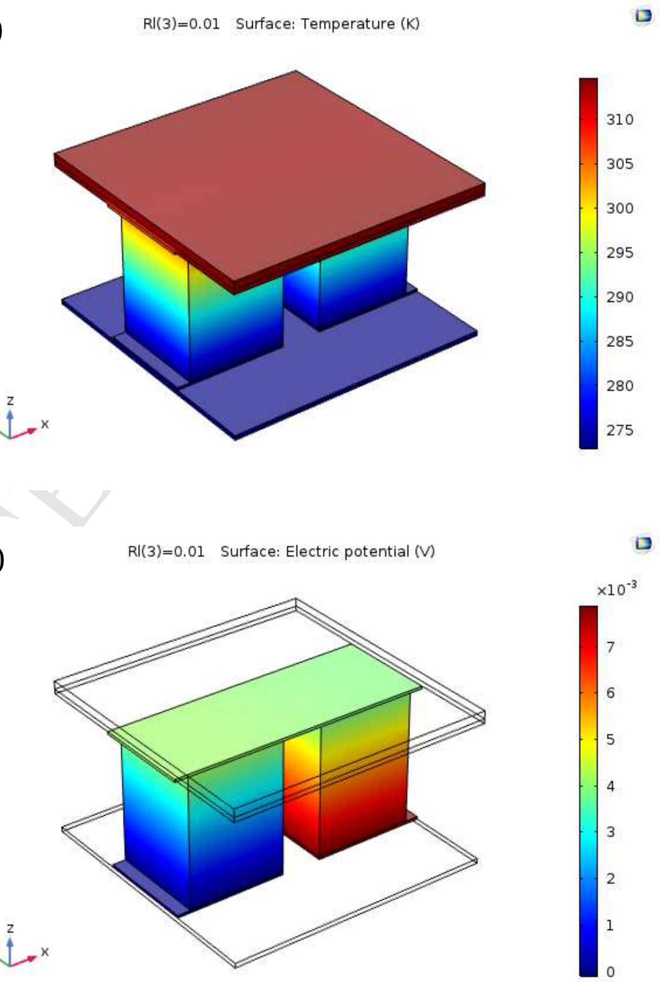

Fig. 6. PV-TE 3-dimensional a) Temperature and b) Voltage distributions for $R_A = 1$.

a)

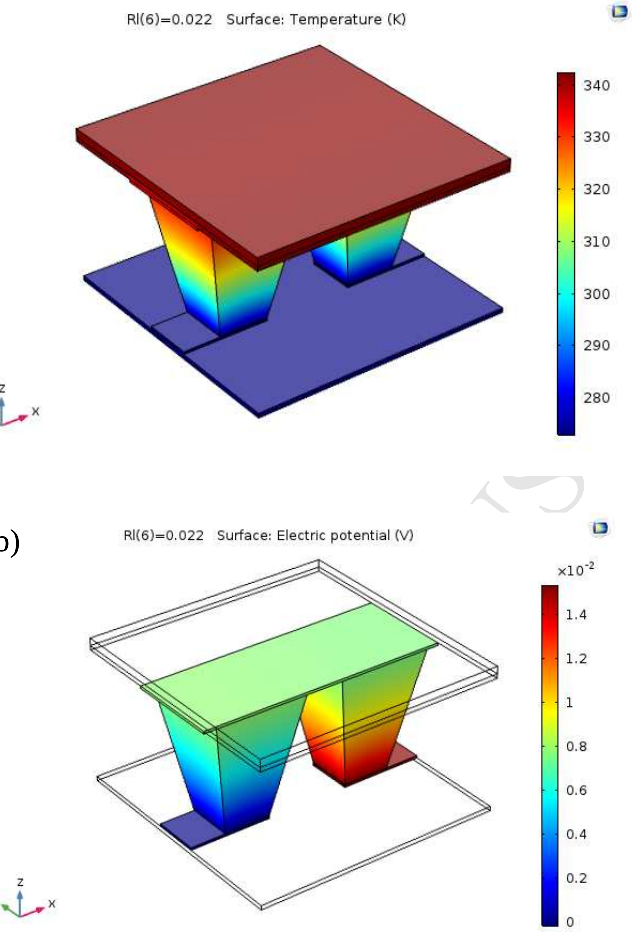

b)

Fig. 7. PV-TE 3-dimensional a) Temperature and b) Voltage distributions for $R_A = 2$.

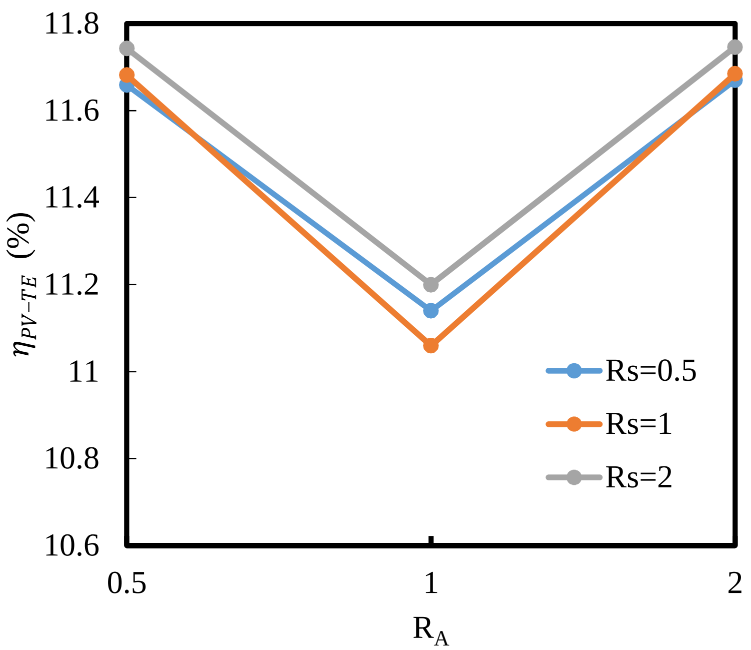

Fig. 8. Overall PV-TE efficiency vs geometry area ratios for Cell A.

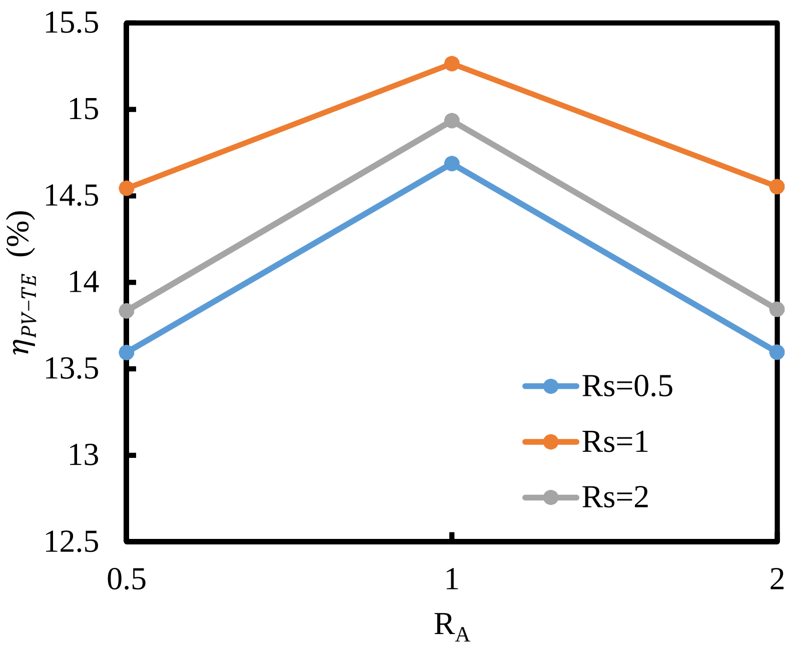

Fig. 9. Overall PV-TE efficiency vs geometry area ratios for Cell B.

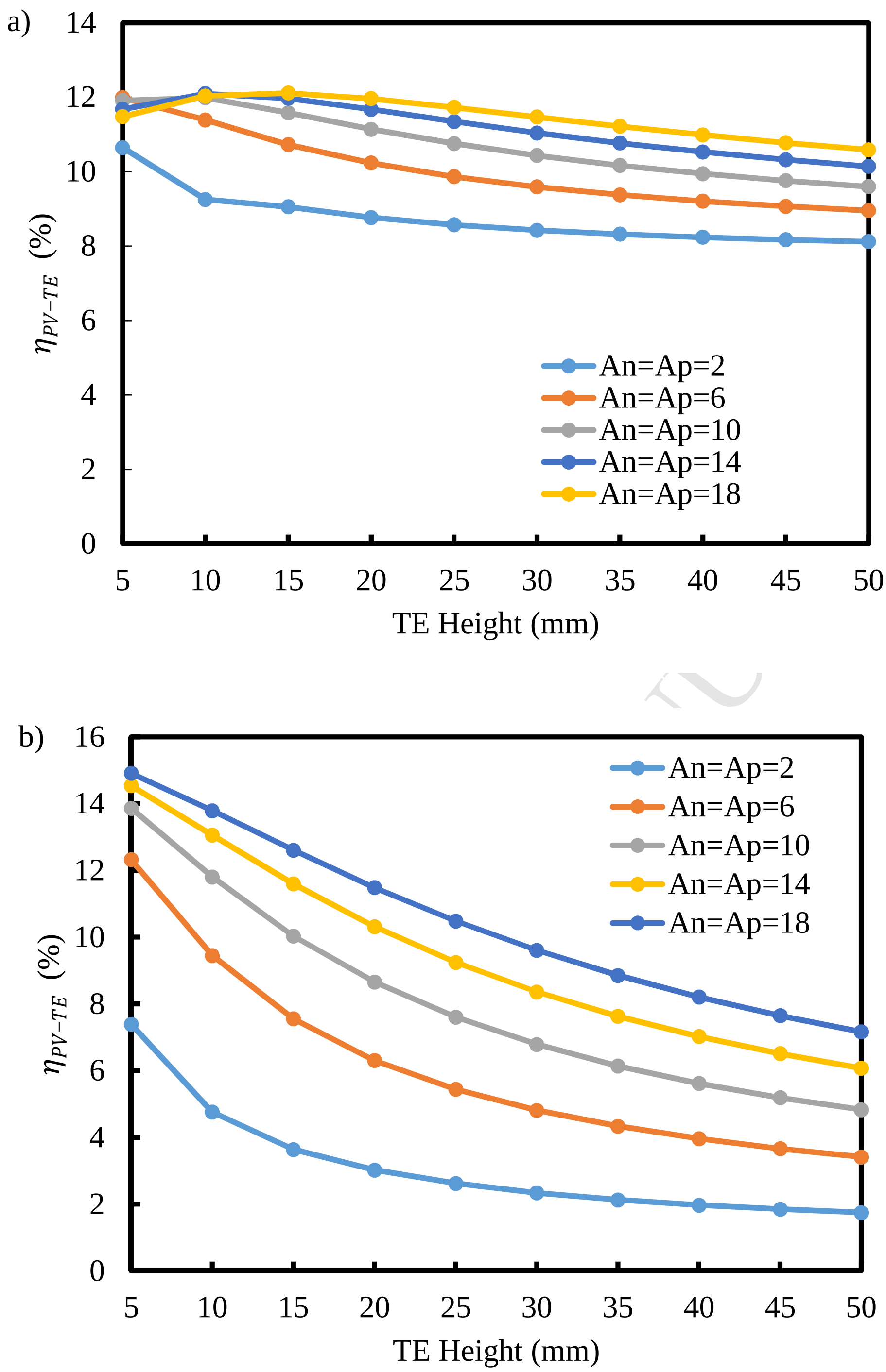

Fig. 10. Hybrid system efficiency vs thermoelectric element height for $R_A = 0.5$ and a) Cell A b) Cell B.

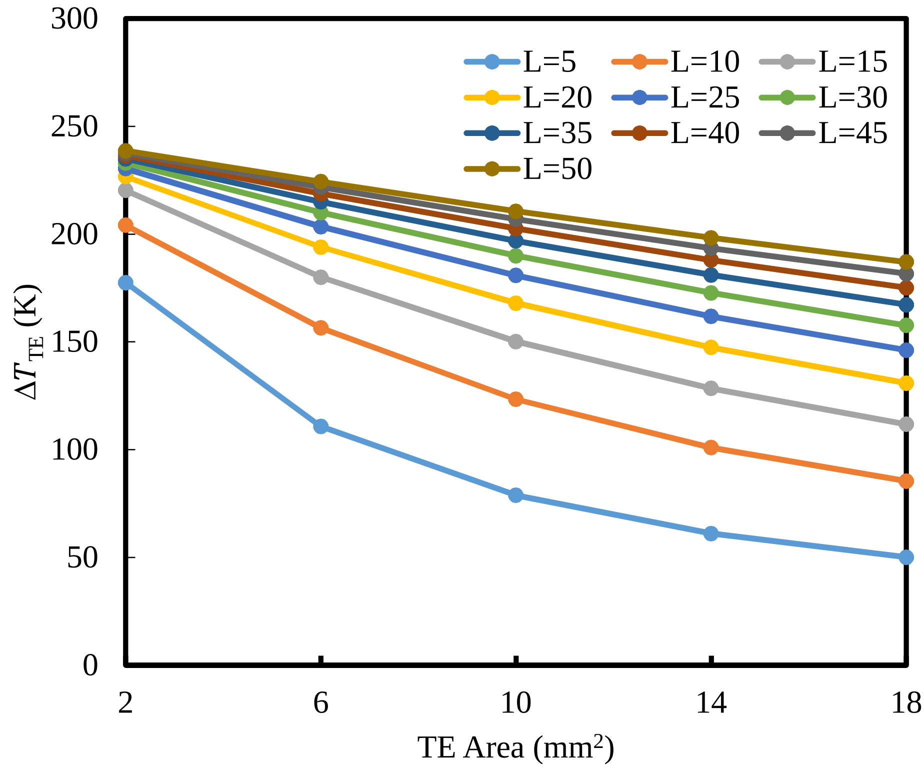

Fig. 11. Thermoelectric temperature difference vs thermoelectric area for $R_A = 0.5$ and both PV cells (Cell A and Cell B).

a)

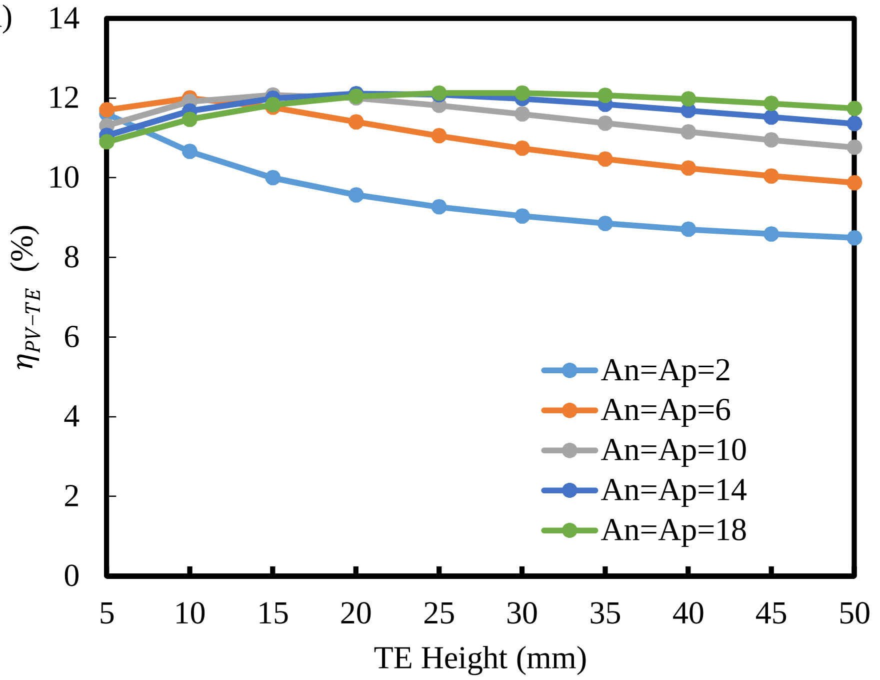

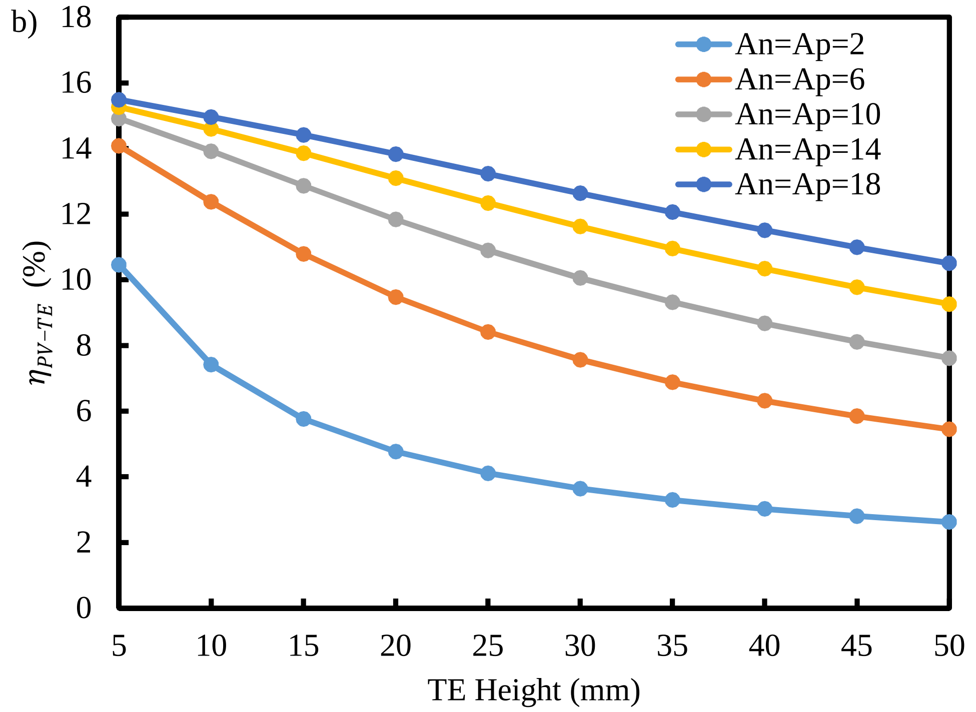

Fig. 12. Hybrid system efficiency vs thermoelectric element height for $R_A = 1$ and a) Cell A b) Cell B.

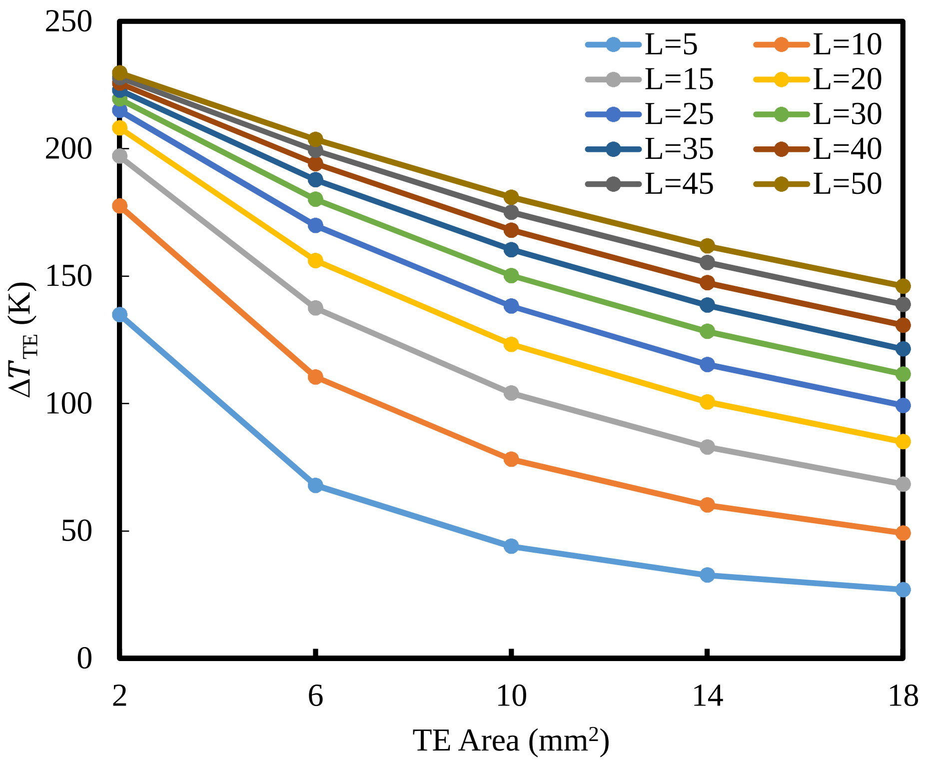

Fig. 13. Thermoelectric temperature difference vs thermoelectric area for $R_A = 1$ and both PV cells (Cell A and Cell B).

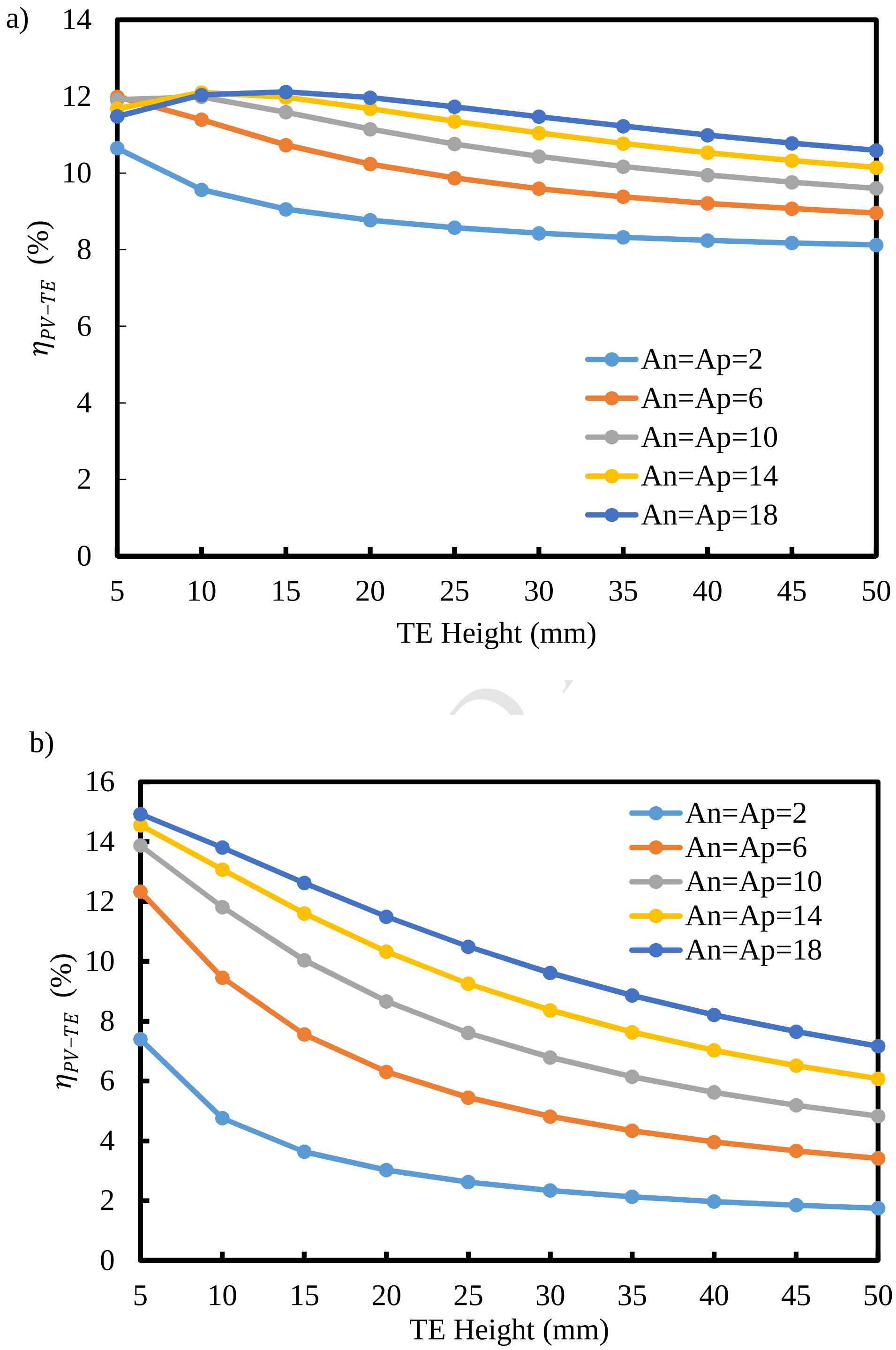

Fig. 14. Hybrid system efficiency vs thermoelectric element height for $R_A = 2$ and a) Cell A b) Cell B.

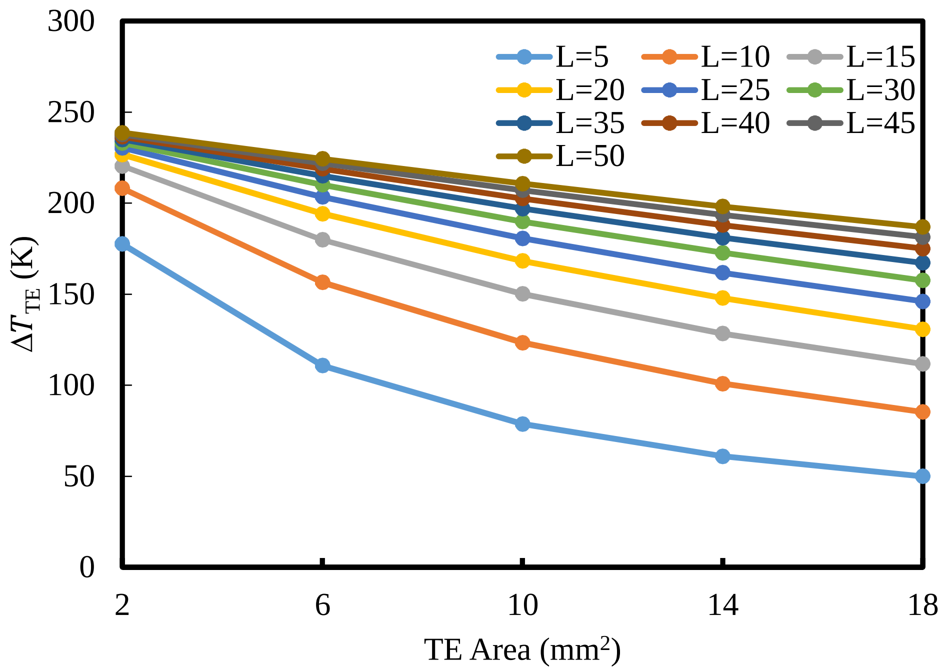

Fig. 15. Thermoelectric temperature difference vs thermoelectric area for $R_A = 2$ and both PV cells (Cell A and Cell B).

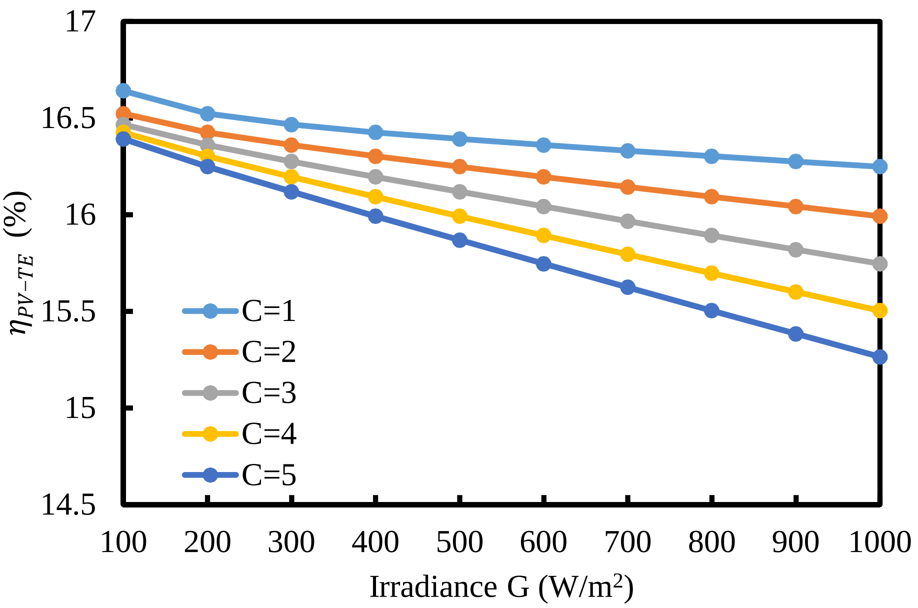

Fig. 16. Hybrid system efficiency vs solar irradiance and concentration ratio.

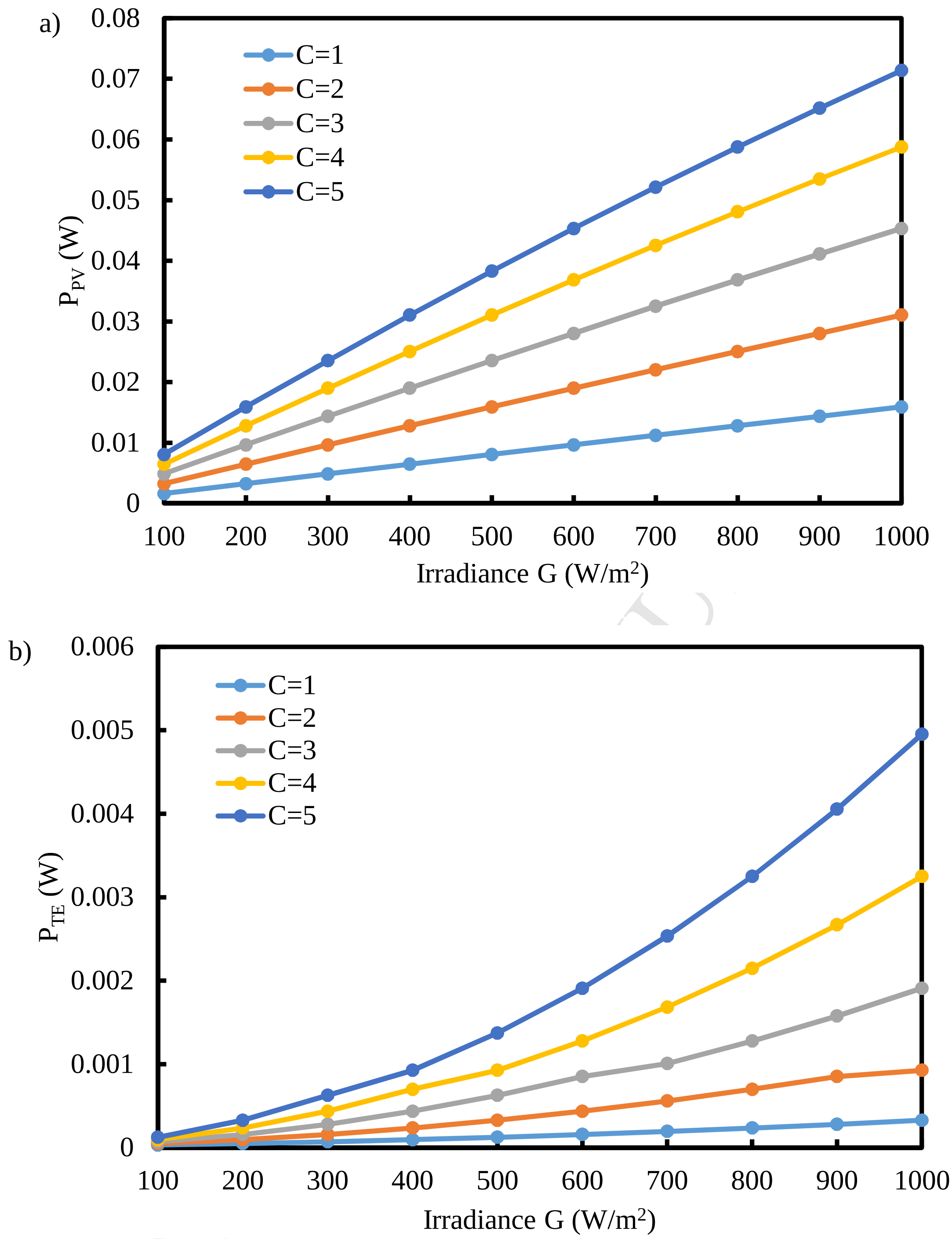

Fig. 17. Variation of a) PV and b) TEG power outputs with solar irradiance and concentration ratio.

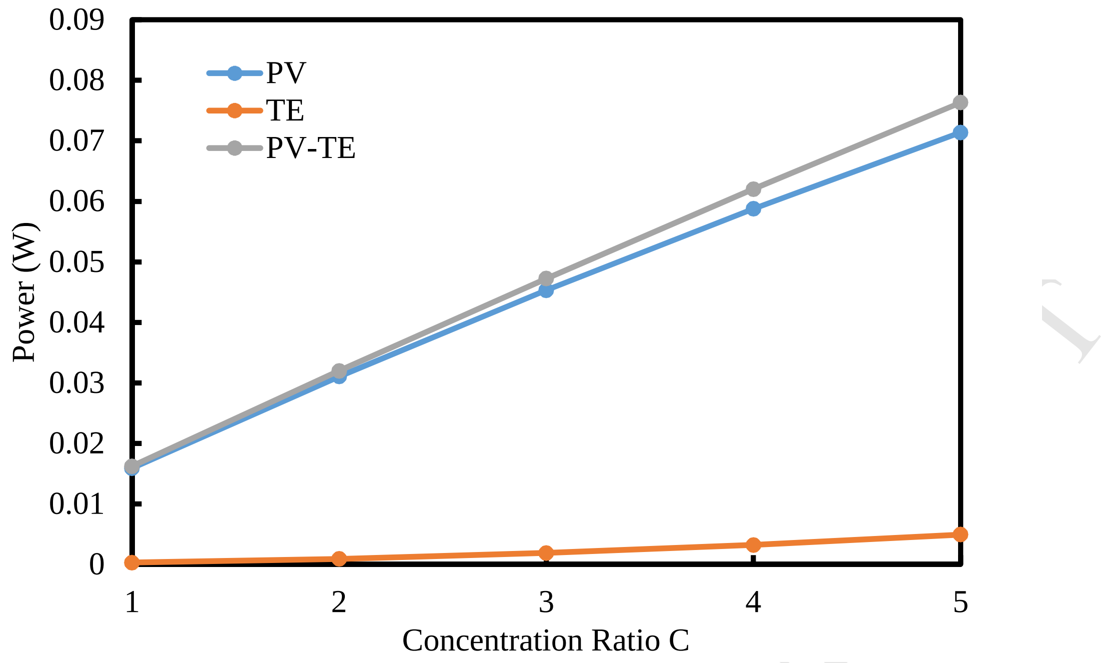

Fig. 18. Variation of PV, TEG and PV-TE power outputs with concentration ratio.

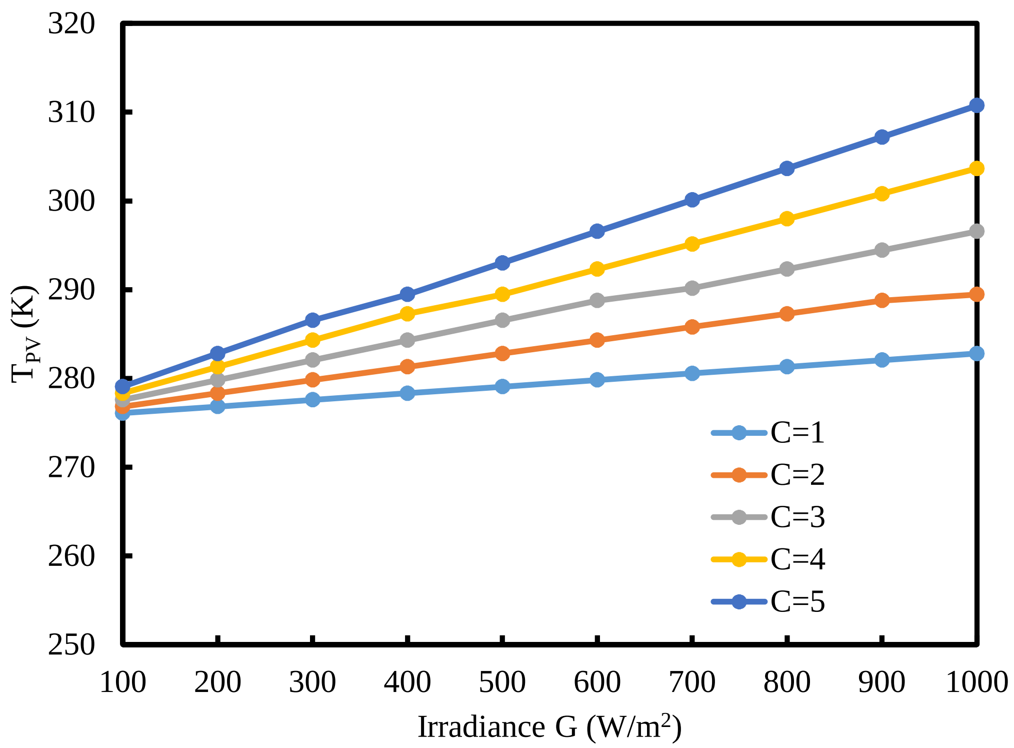

Fig. 19. Variation of PV surface temperature with solar irradiance and concentration ratio for Cell B.

794 **Table 1.** Temperature dependent material properties (T is temperature in K) [43].

	p-type	n-type
Electrical conductivity, $\sigma\ [S/m]$	$(0.015601732T^2 - 15.708052T + 4466.38095) \times 10^2$	$(0.01057143T^2 - 10.16048T + 3113.714229) \times 10^2$
Seebeck coefficient, $S\ [V/K]$	$(-0.003638095T^2 + 2.74380952T - 296.214286) \times 10^{-6}$	$(0.00153073T^2 - 1.08058874T - 28.338095) \times 10^{-6}$
Thermal conductivity, $k\ [W/(m \cdot K)]$	$0.0000361558T^2 - 0.026351342T + 6.22162$	$0.0000334545T^2 - 0.023350303T + 5.606333$

795

796

797 **Table 2.** Material properties [18,20,27].

	Heat capacity, C_p [J/(kgK)]	Density, ρ [kg/m^3]	Seebeck coefficient, S [V/K]	Electrical conductivity, σ [S/m]	Thermal conductivity, k [W/(mK)]
Alumina	900	3900	-	-	27
Bi_2Te_3 (p-n types)	154	7700	$\pm S(T)$ Table 1	$\sigma(T)$ Table 1	$k(T)$ Table 1
Copper	385	8960	-	58100000	401
Silicon (PV)	700	2329	-	-	148
Tedlar	1090	1780	-	-	0.2

798

Table 3. Parameters used in hybrid PV-TE model.

Parameters	Symbol	Value	References
Absorptivity of PV	α_{PV}	0.9	[18]
Ambient temperature	T_{amb}	298 K	[20]
Area of PV	A_{PV}	0.0001 m^2	[31]
Area of TE element	A_{TE}	0.000014 m^2	[33]
Concentration ratio	c	5	[33]
Emissivity of PV	ε_{PV}	0.8	[33]
Heat transfer coefficient	h_{amb}	5 $Wm^{-2}K^{-1}$	[14]
Height of TE element	L	0.005 m	[33]
Solar irradiation	G	1000 W/m^2	[20]
Thickness of copper	H_{cu}	0.0001 m^2	[33]
Thickness of PV	H_{PV}	0.0003 m	[18]
Thickness of tedlar	H_{ted}	0.000175 m	[18]
Wind velocity	u_w	1 m/s	[33]
PV Cell A efficiency at standard test conditions (STC)	η_{PV}	10%	[32]
Cell A temperature coefficient	φ_{PV}	0.001 K^{-1}	[32]
PV Cell B efficiency at standard test	η_{PV}	15%	[46]

conditions (STC)			
Cell B temperature coefficient	φ_{PV}	0.004 K^{-1}	[46]

- Nine geometric configurations and two different solar cells were analysed.
- Two thermoelectric element geometric area ratios were presented.
- Performance of the hybrid system with different factors was analysed.
- Finite element method was used to solve the 3-dimensional heat transfer equations.